POLITECNICO DI TORINO
Repository ISTITUZIONALE

A simplified stress–strain relationship for the mechanical behavior of corroded prestressing strands: The SCPS model

Original
A simplified stress–strain relationship for the mechanical behavior of corroded prestressing strands: The SCPS model / Franceschini, Lorenzo; Belletti, BEATRICE CARLA; Tondolo, Francesco; Sanchez Montero, Javier. - In: STRUCTURAL CONCRETE. - ISSN 1751-7648. - (2022), pp. 189-210. [10.1002/suco.202200170]

Availability:
This version is available at: 11583/2979213 since: 2023-06-06T14:35:17Z

Publisher:
Wiley

Published
DOI:10.1002/suco.202200170

Terms of use:
openAccess

This article is made available under terms and conditions as specified in the corresponding bibliographic description in the repository

Publisher copyright

(Article begins on next page)

12 June 2023

Check for updates

Received: 18 February 2022 | Revised: 17 May 2022 | Accepted: 5 July 2022

DOI: 10.1002/suco.202200170

ARTICLE

fib CEB-FIP WILEY

A simplified stress–strain relationship for the mechanical behavior of corroded prestressing strands: The SCPS-model

Lorenzo Franceschini[1] | **Beatrice Belletti**[2] | **Francesco Tondolo**[3] | **Javier Sanchez Montero**[4]

[1]Department of Engineering and Architecture, University of Parma, Parma, Italy

[2]Structural Engineering at Department of Engineering and Architecture, University of Parma, Parma, Italy

[3]Department of Structural Engineering, Geotechnical and Building Engineering (DISEG), Politecnico di Torino, Torino, Italy

[4]CSIC – at Instituto de Ciencias de la Construction Eduardo Torroja (IETCC), Madrid, Spain

Correspondence
Lorenzo Franceschini, Department of Engineering and Architecture, University of Parma, Parco Area delle Scienze 181/A, 43124 Parma, Italy.
Email: lorenzo.franceschini@unipr.it

Abstract

This article presents a simplified stress–strain relationship for the definition of the mechanical behavior of prestressing strands subjected to chloride-induced corrosion, named SCPS-model (Simplified Model for Corroded Prestressing Strands). The constitutive law adopts the equivalent spring model, that reproduces the overall behavior of a corroded strand by summing the contributions of each wire, assumed as a spring working in parallel to the others. The SCPS-model is designed for the application in the daily engineering practice; to this aim, it is based on a single input parameter that is the maximum penetration depth of the most corroded wire. Following a detailed description of the model formulation and parameters, the article shows the validation of the stress–strain relationship through several comparisons with experimental tensile test outcomes coming from scientific literature. Finally, a statistical analysis of the dimensionless ratio of experimental and analytical results in terms of ultimate corroded strength and strain is carried out to demonstrate the effectiveness of the SCPS-model. Concluding, the accurate and safe side prediction of the residual mechanical behavior of corroded prestressing strands is proposed using the SCPS-model.

KEYWORDS

corrosion, mechanical behavior, pitting, prestressing strands, stress–strain relationship

1 | INTRODUCTION

In the last decades, global warming has become a crucial topic in the international debate. This phenomenon is generally recognized as the main cause triggering natural hazards such as storms, heatwaves, hurricanes, floodings, and so forth. From the engineering point of view, the growth over time in intensity and frequency of such hazards, induced by climate changes, has led to the rising exposure of existing structures and infrastructures to severe structural damages, causing economic and human losses, as reported in the "Global Assessment report".[1] Moreover, the "Making Critical Infrastructure Resilient" report[2] pointed out that the European economic losses related to damages to infrastructure as consequence of extreme weather events (i.e., heavy rains, storms, and snows) amount approximately to €9.3 billion annually and it is

Discussion on this paper must be submitted within two months of the print publication. The discussion will then be published in print, along with the authors' closure, if any, approximately nine months after the print publication.

This is an open access article under the terms of the Creative Commons Attribution License, which permits use, distribution and reproduction in any medium, provided the original work is properly cited.
© 2022 The Authors. *Structural Concrete* published by John Wiley & Sons Ltd on behalf of International Federation for Structural Concrete.

expected to increase up to €37 billion by 2080. In this context, one of the most affected sectors is the transport one with an annual economic loss of about €0.8 billion.

Among the possible extreme natural hazards induced by climate changes, the rise in sea level and heavy snows, can be considered as the major causes affecting chloride-induced corrosion deterioration.[2] According to EN 206,[3] the definition of the exposure classes is strictly related to the proximity of structures and infrastructures from the sea. Therefore, the proper exposure class can vary over time as consequence of climate change leading to more aggressive environments. Moreover, the increase in the frequency of heavy snow events and freeze–thaw cycles, leads to the use of deicing salts more often than in the past to ensure the maintenance and operation of transport lines.

It is worth noting that the evolution process of corrosion phenomenon is closely related to the nature of the surrounding environment—where the structural element is placed. In this regard, chloride-induced corrosion is predominant in marine environments or where the use of de-icing salts is frequent; on the other hand, carbonation-induced corrosion is most likely to occur in places rich in carbon dioxide. In urbanized area, the combination of the exposure to carbon dioxide and chloride ions may cause even worst scenarios.[4]

Considering the detrimental effects associated to corrosion, one of its primary consequences is the reduction of the mechanical properties of reinforcements. In this context, several works have been carried out to investigate the stress–strain relationship of corroded steel rebars,[5–16] whereas limited studies have been performed for the prediction of the residual mechanical response of corroded prestressing strands.[17–22] In Table 1, the main features of each model are summarized. In detail, the several decay laws proposed by different authors are generally based on one of these parameters: (i) the mass loss, η, of the corroded sample, generally evaluated by adopting the procedure described in the ASTM G1-03 Standard,[23] or (ii) the cross-sectional loss, μ, of the corroded prestressing strand. Referring to the in situ measurement and inspection, recent works pointed out that the measurement of the mass loss is unsuitable to carry out due to the need to weight the mass of the residual reinforcement.[18,20,24] On the contrary, the assessment of the minimum residual cross-sectional loss can be obtained by means of non-destructive techniques.[25]

Regardless of the type of corrosion, the reduction of reinforcement cross-section has direct effects on the residual carrying capacity of the structural element. In particular, referring to chloride-induced corrosion, different pit-type morphology configurations were proposed for the evaluation of the cross-sectional loss due to pitting. Val et al.[26] introduced a hemispherical pit-type morphology configuration, Hartt and Lee[27] proposed a planar configuration, whereas Jeon et al.[18] and Franceschini et al.[17] considered three different pit-type morphology configurations to properly describe the variability in shape of pitting corrosion. However, considering the complexity of expressions and the number of parameters involved in the prediction of the residual mechanical response of corroded prestressing strands, the applicability of the constitutive laws reported in Table 1 results hardly applicable in the daily engineering practice.

To this aim, this work introduces a simplified version, named SCPS-model (Simplified Model for Corroded Prestressing Strands), of the stress–strain relationship proposed by the Franceschini et al.[17] According to the SCPS-model, the tensile resistance of corroded prestressing strands depends only on the value of the maximum penetration depth of the most corroded wire, P_{max}, which can be easily measurable during in situ inspections.

Firstly, to overcome the issues related to the time-consuming procedure carried out for the identification of the most suitable shape caused by pitting corrosion, the SCPS-model is conceived to be independent from the possible pit-type morphology configurations. Simplified expressions for the prediction of the corroded ultimate strain and the residual cross-section of the corroded wire are introduced as a function of a single parameter P_{max}/r_{outer}, that is the ratio between the maximum penetration depth, P_{max}, of the most corroded wire and the initial uncorroded radius of the external wire, r_{outer}. Secondly, starting from the measured maximum penetration depth, an average penetration depth, P_{av}, is attributed to the remaining five external wires, while—based on experimental evidence—the inner wire is assumed as uncorroded.

Thirdly, the equivalent spring model is adopted for the description of the residual tensile behavior of a corroded seven wires prestressing strand. Finally, the accuracy and the reliability of SCPS-model are statistically validated by comparing the outcomes of the analytical stress–strain relationships with the experimental tensile test results reported in Franceschini et al.[17] and Jeon et al.[18]

To conclude, the improvement introduced by the SCPS-model consists in providing a useful tool for engineers in current practice, which is characterized by a high qualitative and quantitative prediction of the residual tensile response of corroded prestressing strands. Moreover, unlike all the models available in scientific literature (Table 1), the SCPS-model does not require the estimation of hardly measurable input parameters during in situ inspection such as the pit-type morphology configuration—and the consequent evaluation of the cross-sectional loss, μ—or the mass loss, η.

2 | CHARACTERIZATION OF CORRODED STRANDS

In this section, the characterization of the analyzed prestressing strands is illustrated.

17517648, 2023, 1, Downloaded from https://onlinelibrary.wiley.com/doi/10.1002/suco.202200170 by Politecnico Di Torino Sist. Bibl Del Polit Di Torino, Wiley Online Library on [06/06/2023]. See the Terms and Conditions (https://onlinelibrary.wiley.com/terms-and-conditions) on Wiley Online Library for rules of use; OA articles are governed by the applicable Creative Commons License

TABLE 1 Summary of scientific literature studies on the mechanical behavior of corroded prestressing strands

Constitutive law Main features	Lu et al.[19]	Zhang et al.[21]	Zhang et al.[22]	Jeon et al.[18]	Wang et al.[20]	Franceschini et al.[17]	Franceschini et al.[17] SCPS-model
Experimental program							
Number of tested samples	2 references/ 12 corroded	3 references/7 corroded	Tests on wires	3 references/13 corroded	1 reference/18 corroded	4 reference/19 corroded	Franceschini et al.[17]
Equivalent diameter of strands [mm]	15.2	15.2	15.2	15.2	15.2	12.9	12.9
Type of corrosion	Artificial: Impressed current	Artificial: Climate box	Artificial: Impressed current	Natural: Chloride	Artificial: Climate box	Natural: Chloride	Natural: Chloride
Characteristics of artificial corrosion	100 [$\mu A/cm^2$]	Salt fog (5% salt solution)	100 [$\mu A/cm^2$]	X	By using a wet sponge: 120 min on to 120 min off	X	X
Maximum strand/ wire section loss [%]	Strand: 20.4%	Strand: 27.5%	Wire: 31.4%	Wire: 20.3%	Strand: 27.5%	Wire: 69.20%	Franceschini et al.[17]
Tensile test: test speed	0.2 kN/s	1 mm/min until failure first wire; 2 mm/min for the residual capacity	—	5 mm/min	1 mm/min	Displacement control method	Franceschini et al.[17]
Constitutive law: stress–strain relationship							
Main parameter of the model	Section loss (strand)	Section loss (strand)	Section loss (wire)	Section loss (wire)	Section loss (strand)	Section loss (wire)	Maximum penetration depth
Elasticity modulus variability	V	X	X	X	X	X	X
Critical cross-sectional loss/ mass loss/P_{max}/ r_{outer}	8%	11%	8%	From 3.6% to 8.1% for pit morphologies	10.4%	Pit morphology 1: 8.1% Pit morphology 2: 10.7% Pit morphology 3: 5.4%	$P_{max}/r_{outer} = 0.33$
Regression trend: ultimate strain	Exponential	Linear in intervals	Linear in intervals	Exponential in intervals	Linear in intervals	Exponential in intervals	Linear in intervals
Regression trend: ultimate strength	Linear	Linear in intervals (X)	Linear	Linear	Linear in intervals	Exponential	Linear in intervals (X)
Type of stress–strain relation	Bilinear	Bilinear	Bilinear	Bilinear	Bilinear	Trilinear	Trilinear
Model validation	V	V	V	V	V	V	V

17517648, 2023, 1, Downloaded from https://onlinelibrary.wiley.com/doi/10.1002/suco.202200170 by Politecnico Di Torino Sist. Bibl Del Polit Di Torino, Wiley Online Library on [06/06/2023]. See the Terms and Conditions (https://onlinelibrary.wiley.com/terms-and-conditions) on Wiley Online Library for rules of use; OA articles are governed by the applicable Creative Commons License

Initially, the material properties and the geometrical features of the naturally corroded prestressing strands retrieved from 10 year-old PC beams are outlined. Then, the measurement procedure of the fundamental parameter of the model, which is the maximum penetration depth, P_{max}, of the most corroded wire, is briefly described. Last, the residual mechanical properties of corroded prestressing strands are evaluated through tensile tests.

2.1 | Retrieval of samples and corrosion measurements

A total of 23 prestressing strands, characterized by different levels of corrosion, were retrieved from 10 year-old naturally corroded PC beams subjected to wet-dry cycles by using seawater during service life.[28,29] The beams were tested at the Instituto Eduardo Torroja of Madrid. Four samples were classified as uncorroded due to the absence of corrosion damage, whereas the remaining nineteen showed different corrosion levels and clear localized corrosion (pitting corrosion) characterized by the presence of various pits of different longitudinal and transv dimensions and depths (Figure 1).

The prestressing strands have an equivalent diameter equal to 12.9 mm and are made up of seven wires. The six external wires have a diameter, ϕ_{outer}, equal to 4.26 mm ($r_{outer} = 2.13$ mm), leading to a cross-section, $A_{w,outer,0}$, of about 14.22 mm^2, whereas the inner wire has a diameter, ϕ_{inner}, equal to 4.38 mm ($r_{inner} = 2.19$ mm), leading to a cross-section, $A_{w,inner,0}$, of about 15.00 mm^2.

The samples are identified according to a code where, PB means prestressed beam, the following number—ranging from 9 to 14—stands for the name of the reference beam; then, a letter (L or R) is added to specify the cross-sectional position of the retrieved strand; last, the numbers in brackets represent the initial and final abscissa of the position of the sample along the entire length of the beam, as reported in Table 2.[17,30]

Then, after the cleaning phase that consisted in the removal of rust products according to the procedure described in the ASTM G1-03 Standard,[23] the 3D scanning of corroded and uncorroded strands was performed by means of the ATOS Compact structured light 3D scanner (Figure 1). The powerfulness of this approach consists in the creation of accurate 3D models, that can reproduce the morphology of each pit characterizing the corroded strand with high level of approximation. The scanning procedure allowed to measure only the external surface of the external wires, excluding the inner one; nevertheless, after the cleaning phase and the inspection activity—highlighted in Figure 1—carried out on corroded samples retrieved from the PC beams, it was observed that the inner wire and the inner part of external wires were not affected by corrosion deterioration. For this reason, despite the SCPS-model is able to take into account a different level of corrosion for each wire making up the

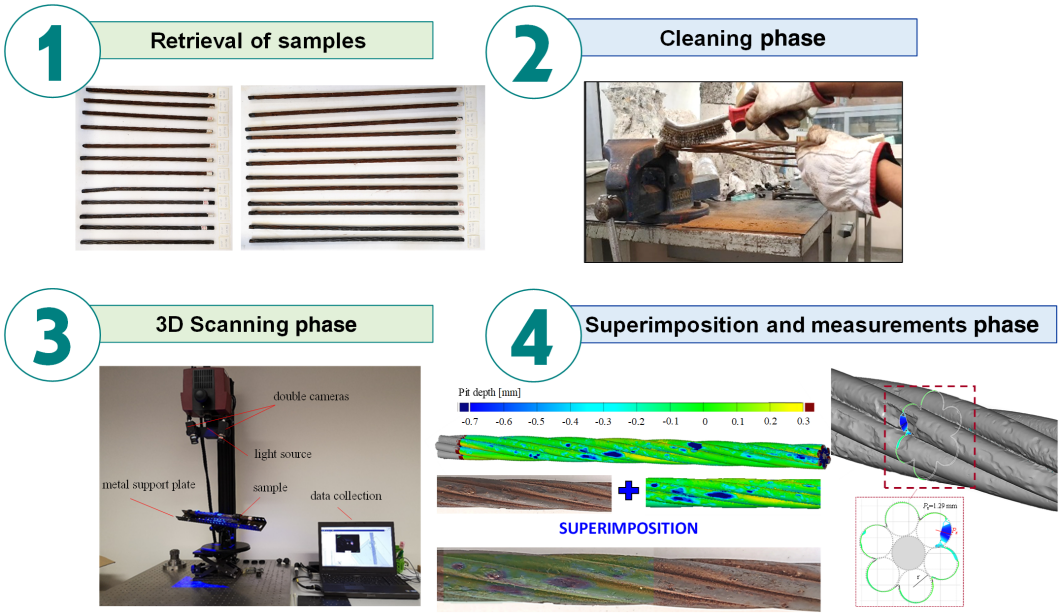

FIGURE 1 Characterization of prestressing strands: Retrieval of samples, cleaning phase and inspection activity, 3D scanning procedure, and superimposition phase and measurements of P_{max}.

17517648, 2023, 1, Downloaded from https://onlinelibrary.wiley.com/doi/10.1002/suco.202201170 by Politecnico Di Torino Sist. Bibl Del Polit Di Torino, Wiley Online Library on [06/06/2023]. See the Terms and Conditions (https://onlinelibrary.wiley.com/terms-and-conditions) on Wiley Online Library for rules of use; OA articles are governed by the applicable Creative Commons License

TABLE 2 Prestressing strands: (i) sample ID, (ii) main geometrical features (P_{max}, P_{av}), and (iii) main parameter for the prediction of the decay trend of the ultimate corroded strain (P_{max}/r_{outer})

Present research and Franceschini et al.[17]				Jeon et al.[18]			
Sample ID[a]	P_{max} [mm]	P_{max}/r_{outer} [−]	P_{av}/r_{outer} [−]	Sample ID[b]	P_{max} [mm]	P_{max}/r_{outer} [−]	P_{av}/r_{outer} [−]
PB9-L(12–82)	1.711	0.800	0.445	NCS	Not corroded	—	—
PB9-L(426–496)	0.424	0.200	0.065	CS1	0.280	0.112	0.033
PB9-R(15–60)	2.784	1.310	0.973	CS2	0.170	0.068	0.019
PB9-R(428–473)	Not corroded	—	—	CS3	0.800	0.320	0.119
PB10-L(138–208)	0.590	0.280	0.098	CS4	1.450	0.580	0.272
PB10-L(445–515)	2.447	1.150	0.786	CS5	0.610	0.244	0.083
PB10-R(287–332)	2.880	1.350	1.029	CS6	0.720	0.288	0.103
PB11-L(5–75)	Not corroded	—	—	CS7	0.900	0.360	0.139
PB11-L(196–266)	1.402	0.660	0.328	CS8	0.410	0.164	0.051
PB11-R(6–51)	0.976	0.460	0.194	CS9	0.980	0.392	0.156
PB11-R(273–318)	1.260	0.590	0.280	CS10	0.400	0.160	0.050
PB12-L(12–82)	1.550	0.730	0.382	CS11	0.110	0.044	0.012
PB12-L(124–169)	1.227	0.580	0.269	CS12	0.359	0.144	0.044
PB12-R(100–170)	1.040	0.490	0.212				
PB12-R(358–403)	Not corroded	—	—				
PB13-L(1–46)	1.161	0.550	0.249				
PB13-L(108–178)	1.840	0.860	0.498				
PB13-R(0–70)	1.380	0.650	0.321				
PB13-R(70–115)	1.090	0.510	0.227				
PB14-L(10–55)	2.237	1.050	0.679				
PB14-L(455–500)	Not corroded	—	—				
PB14-R(2–72)	1.227	0.580	0.269				

[a]As in Franceschini et al.[17] samples PB10-R(32–102) and PB14-R(77–122) are neglected.
[b]As in Jeon et al.[18] sample CS13 is neglected, since the stress–strain response is not reported in the original article.

strand—in this case study—the inner wire is assumed as uncorroded as demonstrated by the experimental finding.

Finally, the damage induced by corrosion was detected by superimposing the uncorroded and corroded 3D models elaborated by using GOM-Inspect software; an example is reported in Figure 1. This phase allowed the measurement of the relevant parameter useful to define the stress–strain relationship of corroded prestressing strands that is the maximum penetration depth, P_{max}, of the most corroded wire (Table 2).

2.2 | Residual mechanical response of corroded strands from tensile tests

To investigate the experimental stress–strain response of corroded and uncorroded prestressing strands, mechanical tensile tests were carried out at the Politecnico of Turin by using a universal testing machine with maximum capacity of 250 kN. Before the tests, a high-contrast speckle pattern was applied on the external surface of each sample in a region of interest delimited by the clamps of the tensile machine, with the aim to perform the digital image correlation (DIC) methodology. The tensile tests were performed by adopting a displacement control method that consisted in the loading of samples until the occurrence of failures of wires. Concurrently, a photo recording at each time step was taken by means of a high-resolution digital camera Nikon D90. After the tests, the DIC was performed by using the open-source software package Ncorr[31,32] with the purpose to estimate the strain field of each sample taken into account. More details on the tensile tests procedure and DIC analysis can be found in Franceschini et al.[17] Finally, the experimental tensile force–strain curve for each sample tested was obtained, showing the experimental sequence of tensile failures of each wire making up the corroded strand.

17517648, 2023, 1, Downloaded from https://onlinelibrary.wiley.com/doi/10.1002/suco.202200170 by Politecnico Di Torino Sist. Bibl Del Polit Di Torino, Wiley Online Library on [06/06/2023]. See the Terms and Conditions (https://onlinelibrary.wiley.com/terms-and-conditions) on Wiley Online Library for rules of use; OA articles are governed by the applicable Creative Commons License

TABLE 3 SCPS-model validation: (i) comparison between analytical prediction and experimental outcomes, and (ii) statistical analysis of dimensionless results in terms of ultimate strength and ultimate strain

Sample ID	$T_{pu,cor,exp}$ [kN]	$f_{pu,cor,exp}$ [MPa]	$\varepsilon_{pu,cor,exp}$ [−]	$T_{pu,cor,analytical}$ [kN]	$f_{pu,cor,analytical}$ [MPa]	$\varepsilon_{pu,cor,analytical}$ [−]	$f_{pu,cor,exp}/f_{pu,cor,analytical}$ [−]	$\varepsilon_{pu,cor,exp}/\varepsilon_{pu,cor,analytical}$ [−]
PB9-L(12–82)	118.69	1186.90	0.0068	114.40	1140.00	0.0071	1.04	0.96
PB9-L(426–496)	179.90	1799.00	0.0316	173.21	1726.60	0.0263	1.04	1.20
PB9-R(15–60)[a]	108.20	1082.00	0.0059	48.07	479.18	0.0041	2.26	1.44
PB9-R(428–473)	188.00	1880.00	0.0500	190.18	1901.75	0.0510	0.99	0.98
PB10-L(138–208)	166.70	1667.00	0.0107	166.22	1656.89	0.0165	1.01	0.65
PB10-L(445–515)	94.40	944.03	0.0056	67.00	677.84	0.0050	1.41	1.12
PB10-R(287–332)	69.60	696.00	0.0036	43.22	430.85	0.0039	1.62	0.92
PB11-L(5–75)	187.10	1871.00	0.0513	190.18	1901.75	0.0510	0.98	1.01
PB11-L(196–266)	151.60	1516.00	0.0082	130.40	1299.90	0.0080	1.17	1.03
PB11-R(6–51)	164.20	1642.00	0.0095	149.37	1488.90	0.0092	1.10	1.04
PB11-R(273–318)	138.70	1387.00	0.0075	136.69	1362.60	0.0084	1.02	0.89
PB12-L(12–82)	118.50	1185.00	0.0069	122.79	1224.00	0.0076	0.97	0.91
PB12-L(124–169)	149.10	1491.00	0.0081	135.91	1354.70	0.0085	1.10	0.95
PB12-R(100–170)	149.20	1492.00	0.0086	144.28	1438.20	0.0090	1.04	0.96
PB12-R(358–403)	189.30	1893.00	0.0541	190.18	1901.75	0.0510	1.00	1.06
PB13-L(1–46)	156.20	1562.00	0.0103	140.80	1403.50	0.0087	1.11	1.18
PB13-L(108–178)[a]	86.10	861.00	0.0047	107.48	1071.40	0.0068	0.80	0.69
PB13-R(0–70)	138.10	1381.00	0.0077	131.23	1308.10	0.0081	1.06	0.95
PB13-R(70–115)	156.20	1562.00	0.0084	143.97	1435.10	0.0089	1.09	0.94
PB14-L(10–55)	123.90	1239.00	0.0062	95.05	947.02	0.0063	1.31	0.98
PB14-L(455–500)	196.30	1963.00	0.0484	190.18	1901.75	0.0510	1.03	0.95
PB14-R(2–72)	145.20	1452.00	0.0080	137.24	1368.00	0.0085	1.06	0.94
NCS	259.32	1865.00	0.0750	259.32	1865.00	0.0750	1.00	1.00
CS1	258.28	1857.53	0.0655	245.95	1769.10	0.0529	1.05	1.24
CS2	261.52	1880.82	0.0694	251.19	1806.90	0.0616	1.04	1.13
CS3	235.19	1691.42	0.0149	220.60	1586.80	0.0119	1.07	1.25
CS4[a]	231.97	1668.31	0.0128	195.15	1403.70	0.0089	1.19	1.43
CS5	241.91	1739.79	0.0177	229.97	1654.20	0.0268	1.05	0.66
CS6	240.42	1729.03	0.0201	224.56	1615.30	0.0182	1.07	1.10
CS7	219.77	1573.04	0.0093	214.72	1544.55	0.0098	1.02	0.96
CS8	262.82	1890.20	0.0365	239.68	1724.10	0.0427	1.10	0.85
CS9	232.31	1670.72	0.0108	211.33	1520.10	0.0096	1.10	1.13
CS10	256.51	1844.79	0.0435	240.16	1727.50	0.0435	1.07	1.00
CS11	263.90	1897.91	0.0562	254.04	1827.40	0.0663	1.04	0.85
CS12	266.84	1919.07	0.0597	242.10	1741.50	0.0467	1.10	1.28
						Average, μ	1.09	1.00
						SD, σ	0.130	0.147
						CV [%]	11.98	14.65
						CoC [−]	0.942	0.979

Abbreviations: CoC, coefficient of correlation; CV, coefficient of variation.

[a]Samples considered as outliers and not accounted in the statistical analysis.

17517648, 2023, 1, Downloaded from https://onlinelibrary.wiley.com/doi/10.1002/suco.202200170 by Politecnico Di Torino Sist. Bibl Del Polit Di Torino, Wiley Online Library on [06/06/2023]. See the Terms and Conditions (https://onlinelibrary.wiley.com/terms-and-conditions) on Wiley Online Library for rules of use; OA articles are governed by the applicable Creative Commons License

Thereafter, the corresponding experimental stress–strain curve was determined by dividing the experimental tensile force values, $T_{pu,exp}$, for the uncorroded cross-section of the overall strand, $A_{strand,0}$, which is equal to 100 mm^2, to avoid uncertainties related to the assessment of the effective strand cross-section.

Jeon et al.[18] pointed out that the failure of the corroded prestressing strand is conventionally defined at the rupture of the first wire, which corresponds to the first drop in the experimental stress–strain response. To validate the proposed SCPS-model, the experimental values in correspondence of the latter point are measured in terms of ultimate corroded tensile force, $T_{pu,cor,exp}$, ultimate corroded strain, $\varepsilon_{pu,cor,exp}$, and ultimate corroded strength, $f_{pu,cor,exp}$, and are reported in Table 3 for the further comparison with the analytical predictions. As highlighted in the scientific literature,[17] It is worth noting that the first wire failure generally occurred in correspondence of the most corroded wire, characterized by the maximum penetration depth, P_{max}. Nevertheless, the powerfulness of the proposed model is not limited to the prediction of the first wire failure. Indeed, the overall sectional stress–strain response of each corroded strand at the location of the measured maximum penetration depth is predicted by using the SCPS-model and simplified expressions for the evaluation of the failure sequence of corroded wires are introduced in the following paragraphs as a function of a single input parameter that is P_{max}.

For the sake of clarity, Figure 2 shows the experimental stress–strain curves of corroded and uncorroded prestressing strands. Referring to Figure 2, with the increase of the level of corrosion, the reduction in terms of both ultimate strength and ultimate strain increases. In particular, the uncorroded and slightly corroded strands show a plastic behavior as confirmed by the presence of a hardening phase; whereas the highly corroded ones exhibit a brittle behavior, failing prematurely in the elastic phase, as highlighted in the red-box of Figure 2.

3 | MECHANICAL BEHAVIOR OF CORRODED PRESTRESSING STRANDS

According to the flowchart reported in Figure 3, the main steps and simplifications at the basis of the SCPS-model (Figure 3, right side) are listed in the following and compared with the assumptions governing the CPS-model (Figure 3, left side) previously proposed by Franceschini et al.[17]:

I. **Input parameters.** Both the CPS-model and the SCPS-model are able to consider different levels of corrosion for each wire making up the prestressing strand. For both models the friction behavior between the wires is neglected.
   Input parameters of CPS-model are the maximum penetration depths of each corroded external wires, $P_{max,i}$.
   Input parameter of SCPS-model is the maximum penetration depth of the most corroded wire, P_{max}, only. Starting from this measured value, an average penetration depth, P_{av}, is then attributed to the remaining five external wires based on experimental sectional analyses;
II. **Hardening phase.** The CPS-model limits the development of the hardening phase—in the stress–strain response of a corroded wire—in correspondence of a critical cross-sectional value, μ_{lim}, evaluated as a function of the pit-type morphology

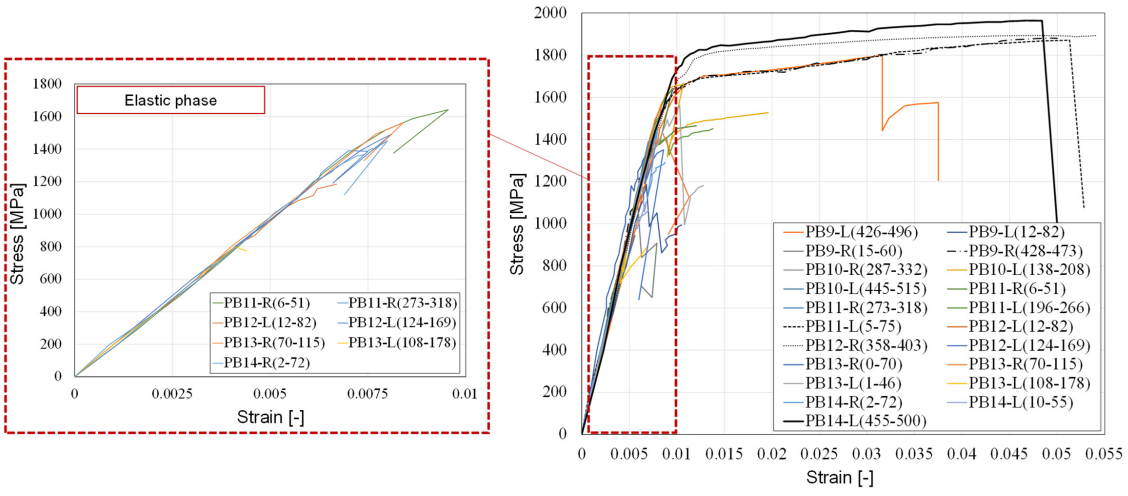

FIGURE 2 Mechanical responses of corroded and uncorroded strands, in black the uncorroded samples.

17517648, 2023, 1, Downloaded from https://onlinelibrary.wiley.com/doi/10.1002/suco.202201170 by Politecnico Di Torino Sist. Bibl Del Polit Di Torino, Wiley Online Library on [06/06/2023]. See the Terms and Conditions (https://onlinelibrary.wiley.com/terms-and-conditions) on Wiley Online Library for rules of use; OA articles are governed by the applicable Creative Commons License

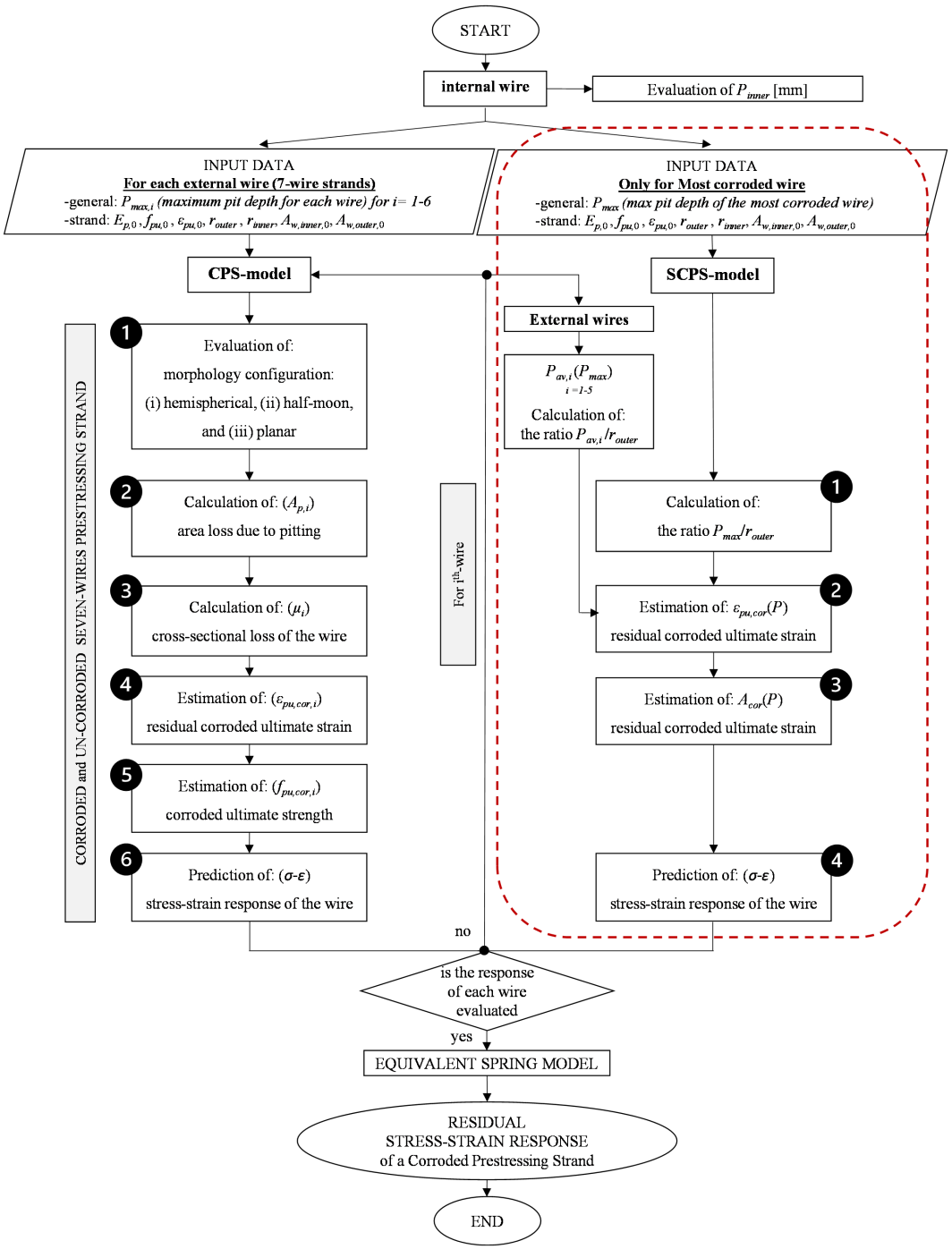

FIGURE 3 Flowchart: Comparison between CPS and SCPS-model.

configurations (resulting equal to 8.1%, 10.7%, and 5.4% for hemispherical, half-moon and planar shape, respectively).

The SCPS-model limits the development of the hardening phase—in the stress–strain response of a corroded wire—in correspondence of a critical value of P_{max}/r_{outer} equal to 0.33 (or 1/6 ϕ_{outer});

III. **Ultimate strain.** The CPS-model evaluates the ultimate strain in correspondence of the ultimate strength calculated as described at point (IV) by adopting exponential relationships—one for each of the three different pit-type morphology configurations—calibrated on experimental tensile tests results carried out on corroded prestressing strands.

The SCPS-model evaluates the ultimate strain by adopting a relationship dependent on P_{max}/r_{outer} values. The stress–strain relationships of corroded

17517648, 2023, 1, Downloaded from https://onlinelibrary.wiley.com/doi/10.1002/suco.202201170 by Politecnico Di Torino Sist. Bibl Del Polit Di Torino, Wiley Online Library on [06/06/2023]. See the Terms and Conditions (https://onlinelibrary.wiley.com/terms-and-conditions) on Wiley Online Library for rules of use; OA articles are governed by the applicable Creative Commons License

wires are the same of the uncorroded one; the only difference consists in the point of interruption in correspondence of the ultimate strain. It results that for slightly corroded wires with a value of P_{max}/r_{outer} lower than the critical value—equal to 0.33—the trilinear relationship with a reduced hardening phase is adopted. For severely corroded wires—with values of P_{max}/r_{outer} ranging from 0.33 to 0.86—a bilinear relationship is adopted. For highly corroded wires—with values of P_{max}/r_{outer} ranging from 0.86 and 2.00—a linear relationship is adopted. The upper boundary limit equal to 2.00 (or ϕ_{outer}) corresponds to the scenario of complete deterioration of the external wire;

IV. **Ultimate strength.** The CPS-model assumes the ultimate strength of each corroded wire dependent on the cross-sectional loss value of each corroded wire, μ_i, which is estimated as a function of the cross-sectional loss due to pitting, $A_{p,i}$, by considering three different pit-type morphology configurations, denoted as: (i) hemispherical shape, (ii) half-moon shape, and planar shape, respectively.

The SCPS-model identifies the ultimate strength in correspondence of the ultimate strain evaluated as described at point (III) by adopting the stress–strain relationship of the uncorroded wire;

V. **Equivalent spring model.** Both the CPS-model and the SCPS-model predict the tensile response of the corroded prestressing strand by adopting the equivalent spring model. Therefore, each wire is considered as a spring working in parallel to the others and the overall response of the strand results from the sum of the responses of each wire.

The CPS-model assumes that the response of each external wire is governed by its own maximum penetration depth and cross-sectional loss of the wire, resulting that the response of each external wire is different and characterized by sequential drop-offs in the stress–strain response.

The SCPS-model assumes that the response of the most corroded wire is governed by the maximum penetration depth, while the response of the remaining external wires is the same and governed by the average penetration depth, estimated as a function of the maximum one. Additionally, a simplified expression for the daily engineering assessment of corroded prestressing strands is evaluated for the SCPS-model;

VI. **Wire cross-section.** The CPS-model calculates the tensile resistance of the corroded wire by multiplying the reduced strength times the value of the cross-section of the uncorroded wire, $A_{w,0}$. Indeed, the corrosion effect is already considered for the evaluation of the strength decay.

The SCPS-model calculates the tensile resistance of the corroded wire by multiplying the reduced strength—as described at point (IV)—times the value of the residual cross-section of the corroded wire, $A_{w,cor}$. Indeed, the reduced strength is estimated as a function of the corroded ultimate strain but does not implicitly take into account the cross-section reduction. To this aim, the SCPS-model evaluates the residual cross-section of the corroded wire by adopting a relationship dependent on P_{max}/r_{outer} values.

VII. **Conventional failure mode.** Both the CPS-model and the SCPS-model can predict the sequence of ruptures of wires during the overall response of the corroded strand, for safe-side engineering assessment, a conventional failure mode is defined in correspondence of the first rupture of the most corroded wire. In the case of refined assessment, both the CPS-model and the SCPS-model can predict the evolutive tensile behavior of the corroded strand after the first rupture of the most corroded wire. In that case, the tensile response of the strand is characterized by a sequence of drop-offs reproducing the sequential rupture of each wire.

3.1 | Mechanical response for uncorroded wire

The stress–strain response of uncorroded wires is reproduced by adopting a trilinear model as reported in Equation (1) and Figure 4[33]:

$$\sigma_w(\varepsilon) = \begin{cases} \varepsilon E_{p,0} & \varepsilon \le \varepsilon_{pp,0} \\ \varepsilon_{pp,0} E_{p,0} + E'_{p,0}(\varepsilon - \varepsilon_{pp,0}) & \varepsilon_{pp,0} < \varepsilon \le \varepsilon_{py,0} \\ \varepsilon_{pp,0} E_{p,0} + E'_{p,0}(\varepsilon_{py,0} - \varepsilon_{pp,0}) + E''_{p,0}(\varepsilon - \varepsilon_{py,0}) & \varepsilon_{py,0} < \varepsilon \le \varepsilon_{pu,0} \\ 0 & \varepsilon > \varepsilon_{pu,0} \end{cases} \quad (1)$$

17517648, 2023, 1, Downloaded from https://onlinelibrary.wiley.com/doi/10.1002/suco.202201170 by Politecnico Di Torino Sist. Bibl Del Polit Di Torino, Wiley Online Library on [06/06/2023]. See the Terms and Conditions (https://onlinelibrary.wiley.com/terms-and-conditions) on Wiley Online Library for rules of use; OA articles are governed by the applicable Creative Commons License

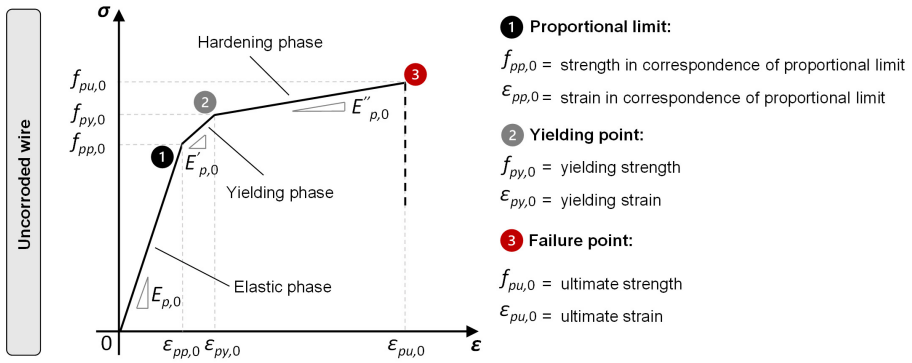

FIGURE 4 Uncorroded mechanical response of wires.

where $\sigma_w(\varepsilon)$ is defined as the stress of a wire with respect to a given ε.

An elastic phase—from (0,0) to ($\varepsilon_{pp,0}$, $f_{pp,0}$)—a yielding phase—from ($\varepsilon_{pp,0}$, $f_{pp,0}$) to ($\varepsilon_{py,0}$, $f_{py,0}$)—and a hardening phase—from ($\varepsilon_{py,0}$, $f_{py,0}$) to ($\varepsilon_{pu,0}$, $f_{pu,0}$) are considered, as reported in Figure 4. In detail, the ultimate uncorroded mechanical properties in terms of ultimate strain, $\varepsilon_{pu,0}$, and ultimate strength, $f_{pu,0}$, are evaluated based on the average values obtained from the four tensile tests carried out on uncorroded prestressing strands, which result equal to 5.1% and 1901.75 MPa, respectively.

The proportional limit ($\varepsilon_{pp,0}$, $f_{pp,0}$) is evaluated as a function of the uncorroded value of the modulus of elasticity, $E_{p,0}$—assumed equal to 195 GPa—and the ultimate uncorroded strength, $f_{pu,0}$. In this context, as suggested by the JCSS,[33] the strength in correspondence of the proportional limit, $f_{pp,0}$, is assumed equal to 0.7 times $f_{pu,0}$, as highlighted in Equation (2), while the corresponding strain (strain in correspondence of the proportional limit), $\varepsilon_{pp,0}$, is calculated as the ratio between $f_{pp,0}$ and the modulus of elasticity, as expressed by Equation (3).

$$f_{pp,0} = 0.7 f_{pu,0} \tag{2}$$

$$\varepsilon_{pp,0} = \frac{f_{pp,0}}{E_{p,0}} \tag{3}$$

Referring to the yielding point ($\varepsilon_{py,0}$, $f_{py,0}$), the yield strength, $f_{py,0}$, is assumed equal to 0.882 times the ultimate uncorroded strength, $f_{pu,0}$, as expressed in Equation (4), whereas a fixed total yield strain, $\varepsilon_{py,0}$, equal to 1% is assumed[33,34]:

$$f_{py,0} = 0.882 f_{pu,0} \tag{4}$$

Finally, the stress–strain response of uncorroded wires is completely defined once the uncorroded yield, $E'_{p,0}$, and hardening modulus, $E''_{p,0}$, are calculated through the expressions reported in Equations (5) and (6), which result equal to 109 and 5.47 GPa, respectively.

$$E'_{p,0} = \frac{f_{py,0} - f_{pp,0}}{\varepsilon_{py,0} - \varepsilon_{pp,0}} \tag{5}$$

$$E''_{p,0} = \frac{f_{pu,0} - f_{py,0}}{\varepsilon_{pu,0} - \varepsilon_{py,0}} \tag{6}$$

3.2 | Main simplifications of the SCPS-model

In this section, the simplified model for the prediction of the residual mechanical response of corroded prestressing strand, SCPS-model, is discussed.

Firstly, the SCPS-model is based on a single input parameter that is the maximum penetration depth, P_{max}, of the most corroded wire. Considering the daily engineering practice, the relevance of this assumption consists in the dependence of the proposed model on a parameter that can be directly measured during in situ inspection by means of technical instrumentation such as the pit depth gauge or a portable laser scanner, without carrying out destructive tests on the existing structural elements. In this context, as pointed out by Yoo et al.,[25] nondestructive methods such as radiography, x-ray, endoscopic inspection, or methods by using magnetic field can be adopted to accurately determine defects in strands along the overall length of a PC element and evaluate the position of the most corroded section. Moreover, Wang et al.[20] identified other possible nondestructive techniques for the evaluation of the corrosion loss of strand such as the acoustic emission method, the half-cell potential, or the linear polarization resistance or visual inspections reporting corrosion stains or corrosion cracks. In this framework, once the position of the minimum cross-sectional loss is known, a local removal of the thickness of the concrete cover allows the measurement of P_{max} by using the pit depth gauge or other technical instruments. Advancement in miniaturized laser scanner techniques is welcomed to this aim also to limit the concrete cover removal around the detected defect with digital measurement of the maximum pit depth other than

17517648, 2023, 1, Downloaded from https://onlinelibrary.wiley.com/doi/10.1002/suco.202200170 by Politecnico Di Torino Sist. Bibl Del Polit Di Torino, Wiley Online Library on [06/06/2023]. See the Terms and Conditions (https://onlinelibrary.wiley.com/terms-and-conditions) on Wiley Online Library for rules of use; OA articles are governed by the applicable Creative Commons License

estimation of outer radius of external wires avoiding gross errors due to the operator measuring activity. Nevertheless, the nondestructive methods are not the main object of the present research and will not be treated further.

Secondly, once P_{max} is measured, an average penetration depth, P_{av}, is attributed to the remaining five external wires by adopting the relationship reported in Equations (7) and (8):

$$\Omega_i = \frac{P_{max}}{2r_{outer}} \frac{\frac{P_{av}}{r_{outer}}}{\frac{P_{max}}{r_{outer}}} = 0.189\left(\frac{P_{max}}{r_{outer}}\right)^2 + 0.125\frac{P_{max}}{r_{outer}} \tag{7}$$

$$\begin{aligned} P_{av} &= 2r_{outer}\Omega_i = 2r_{outer}\left(0.189\left(\frac{P_{max}}{r_{outer}}\right)^2 + 0.125\frac{P_{max}}{r_{outer}}\right) \\ &= r_{outer}\left(0.387\left(\frac{P_{max}}{r_{outer}}\right)^2 + 0.25\frac{P_{max}}{r_{outer}}\right) \end{aligned} \tag{8}$$

where Ω_i is defined as transversal pitting factor, which represents a useful parameter that sectionally correlates the maximum penetration depth of the most corroded wire, P_{max}, and the average penetration depth showed by the remaining external wires, P_{av}. In detail, the relationships expressed in Equations (7) and (8) are derived based on sectional outcomes obtained during the measurement phase carried out by using GOM Inspect software (Figure 5).

The obtained values of P_{av}/r_{outer}—for each corroded prestressing strand analyzed—are reported in Table 2.

As stated before, based on experimental findings—in this case study—the inner wire was observed to be uncorroded. This last assumption can be considered as adequate for limit values of corrosion as reported by experimental activities conducted by the Vecchi et al.[29] Nevertheless, it is worth noting that additional experimental tensile tests on corroded prestressing strand—showing corrosion deterioration of the inner wire—will be performed in order to establish a proper correlation that relates the maximum penetration depth, P_{max}, of the most corroded external wire with the maximum penetration depth of the inner one, P_{inner}.

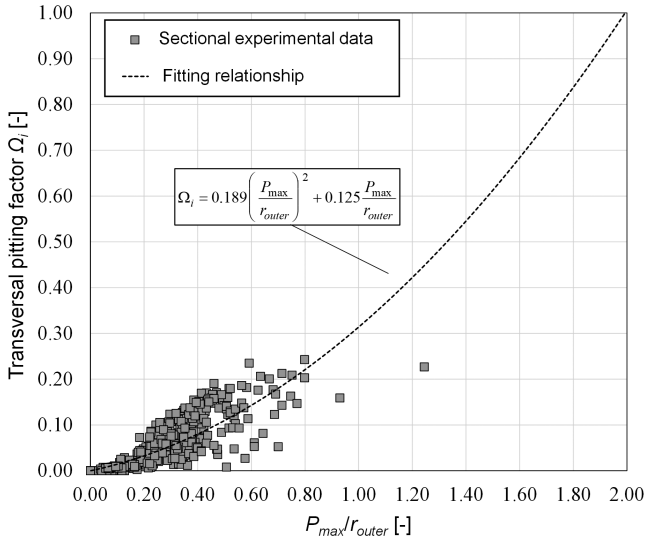

FIGURE 5 Transversal pitting factor Ω_i as a function of the maximum penetration depth, P_{max}.

Thirdly, the ratio P_{max}/r_{outer} between the maximum penetration depth, P_{max}, of the most corroded wire and the initial radius of the external wire, r_{outer} is calculated and reported in Table 2.

Then, Equations (9) and (10) are formulated—regardless of the possible detectable pit-type morphologies and considering the experimental outcomes coming from Franceschini et al.[17] and Jeon et al.[18]—to evaluate the decay of ultimate strain, $\varepsilon_{pu,cor,exp}$, of corroded wires as a function of the ratio P_{max}/r_{outer}. To this aim, referring to the experimental stress–strain (tensile force–strain) relationships obtained from tensile tests, the values of the ultimate corroded strain measured in correspondence of the failure of the most corroded wire were firstly subdivided into two groups: (i) data obtained from samples with the hardening phase in the tensile stress–strain response (denoted as samples having a plastic behavior), and (ii) data obtained from samples without the hardening phase in the tensile stress–strain response (denoted as samples having an elastic behavior). To compare samples coming from different experimental campaigns and characterized by different uncorroded mechanical properties (i.e. $\varepsilon_{pu,0}$ and $\varepsilon_{py,0}$), the dimensionless values of $\varepsilon_{pu,cor}$ for plastic and elastic behavior were calculated, as highlighted in Figure 6. In detail, Figure 6 shows that a critical value of the ratio P_{max}/r_{outer} equal to 0.33—equivalently to 1/6 of the diameter of the external wire, ϕ_{outer}—represents the threshold value beyond which the hardening phase in the stress–strain relationship of a corroded wire disappears, leading to the transition from ductile to brittle failure mode of the wire. Moreover, a lower and an upper boundary limit of the ratio P_{max}/r_{outer} equal to 0 and 2.00 are defined, respectively. The lower boundary limit corresponds to the scenario of uncorroded wire; on the other hand, the upper one corresponds to the scenario when the corrosion phenomenon degrades the whole wire. Since the available experimental outcomes are limited to a P_{max}/r_{outer} ratio equal to 1.40, the last part of the linear trend for P_{max}/r_{outer} ratio that ranges between 1.40 and 2.00 is represented by a dashed line in Figure 6. Furthermore, for values of P_{max}/r_{outer} higher than 1.40, a severe corrosion deterioration of the external wires is expected, which

17517648, 2023, 1, Downloaded from https://onlinelibrary.wiley.com/doi/10.1002/suco.202201170 by Politecnico Di Torino Sist. Bibl Del Polit Di Torino, Wiley Online Library on [06/06/2023]. See the Terms and Conditions (https://onlinelibrary.wiley.com/terms-and-conditions) on Wiley Online Library for rules of use; OA articles are governed by the applicable Creative Commons License

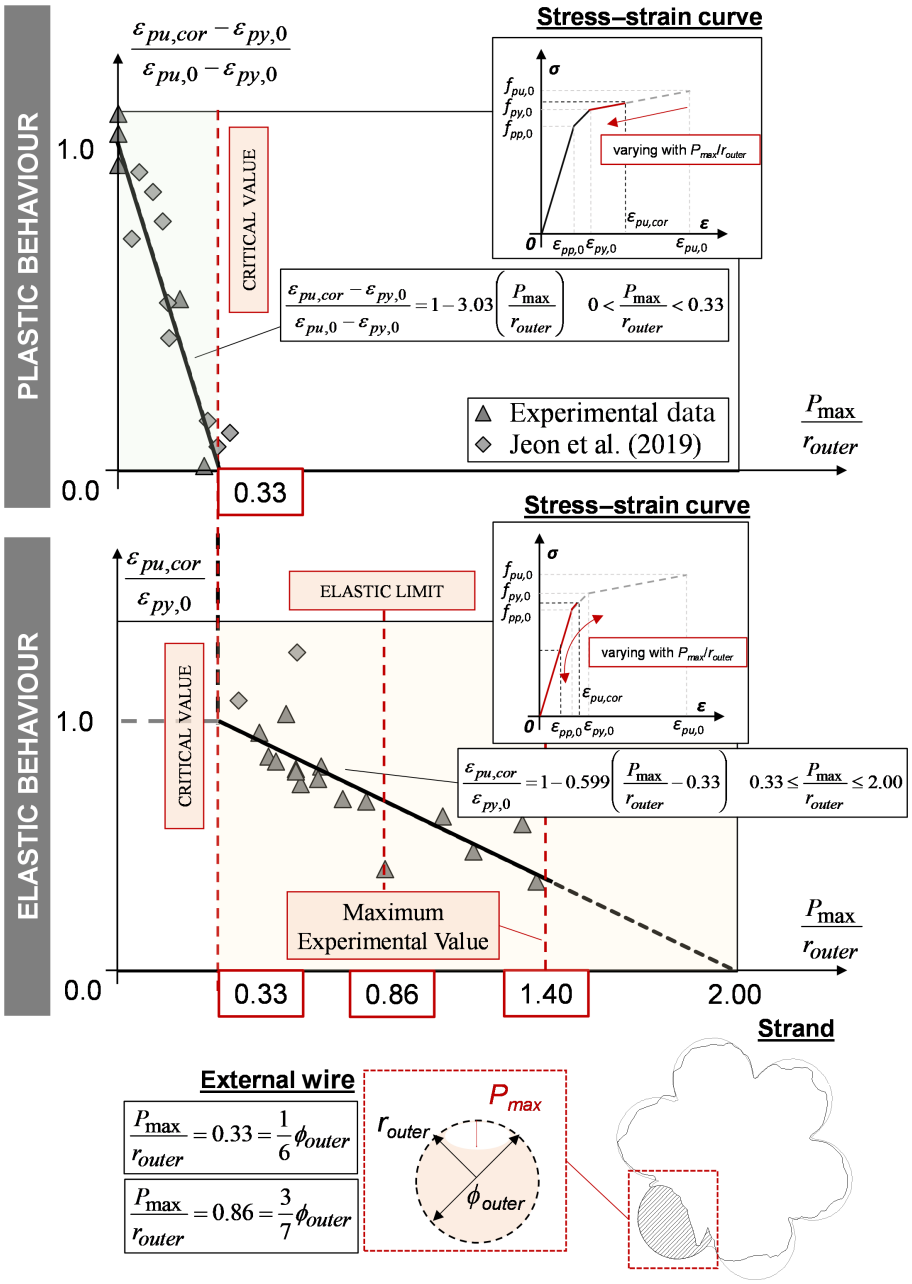

FIGURE 6 Decay trend of ultimate corroded strain.

corresponds to a scenario where the assumption of uncorroded inner wire should be verified through *ad-hoc* experimental tests.

$$\frac{\varepsilon_{\mathrm{pu,cor}}-\varepsilon_{\mathrm{py,0}}}{\varepsilon_{\mathrm{pu,0}}-\varepsilon_{\mathrm{py,0}}}=1-3.03\frac{P_{\max}}{r_{\mathrm{outer}}}\quad 0.00<\frac{P_{\max}}{r_{\mathrm{outer}}}<0.33 \tag{9}$$

$$\frac{\varepsilon_{\mathrm{pu,cor}}}{\varepsilon_{\mathrm{py,0}}}=1-0.599\left(\frac{P_{\max}}{r_{\mathrm{outer}}}-0.33\right)\quad 0.33\le\frac{P_{\max}}{r_{\mathrm{outer}}}\le 2.00 \tag{10}$$

Solving Equations (9) and (10), the value of the ultimate corroded strain, $\varepsilon_{\mathrm{pu,cor}}$, can be directly derived as a function of the ratio $P_{\max}/r_{\mathrm{outer}}$ for the plastic and elastic behavior, respectively, by means of Equations (11) and (12):

$$\varepsilon_{\mathrm{pu,cor}}=\left[\left(1-3.03\frac{P_{\max}}{r_{\mathrm{outer}}}\right)\left(\varepsilon_{\mathrm{pu,0}}-\varepsilon_{\mathrm{py,0}}\right)\right]+\varepsilon_{\mathrm{py,0}}$$

$$0.00<\frac{P_{\max}}{r_{\mathrm{outer}}}<0.33 \tag{11}$$

17517648, 2023, 1, Downloaded from https://onlinelibrary.wiley.com/doi/10.1002/suco.202201170 by Politecnico Di Torino Sist. Bibl Del Polit Di Torino, Wiley Online Library on [06/06/2023]. See the Terms and Conditions (https://onlinelibrary.wiley.com/terms-and-conditions) on Wiley Online Library for rules of use; OA articles are governed by the applicable Creative Commons License

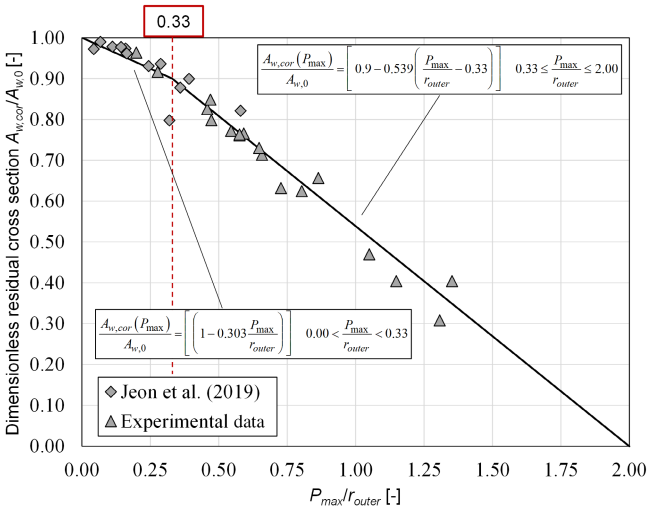

FIGURE 7 Decay trend of residual cross-section.

$$A_{w,cor}(P_{max}) = \left[0.9 - 0.539\left(\frac{P_{max}}{r_{outer}} - 0.33\right)\right] A_{w,0} \quad 0.33 \le \frac{P_{max}}{r_{outer}} \le 2.00 \tag{14}$$

3.3 | Simplified stress–strain relationship for corroded strands

Based on the previous assumptions, the stress of a corroded wire, $\sigma_w(\varepsilon)$, is expressed according to Equation (15) in function of the ratio P_{max}/r_{outer} and the ultimate corroded strain, $\varepsilon_{pu,cor}$, as shown in Figure 8:

According to Equation (15), when the ratio P_{max}/r_{outer} is lower than the critical value ($P_{max}/r_{outer} = 0.33$), the slightly corroded wire experiences a residual hardening phase, leading to a ductile behavior—reproduced by adopting a tri-linear trend of the mechanical response (Figure 8b). Otherwise, when the critical value is exceeded, the hardening phase does not develop, and the severely corroded wire shows a brittle behavior. Referring to the latter, two trends for the description of the residual mechanical response of a corroded wire are considered: (i) for values of the ratio P_{max}/r_{outer} ranging from 0.33 to 0.86, a bilinear trend is adopted (Figure 8c) whereas (ii) for values of the ratio P_{max}/r_{outer} higher than 0.86, the stress–strain relationship collapses in a linear-elastic trend (Figure 8d). Therefore, a further threshold value of P_{max}/r_{outer} equal to 0.86 is considered, which results

$$\sigma_w(\varepsilon) = \begin{cases} \dfrac{P_{max}}{r_{outer}} < 0.33 \\ \varepsilon_{pu,cor} > \varepsilon_{py,0} \end{cases} \begin{cases} \varepsilon E_{p,0} & \varepsilon \le \varepsilon_{pp,0} \\ \varepsilon_{pp,0}E_{p,0} + E'_{p,0}(\varepsilon - \varepsilon_{pp,0}) & \varepsilon_{pp,0} < \varepsilon \le \varepsilon_{py,0} \\ \varepsilon_{pp,0}E_{p,0} + E'_{p,0}(\varepsilon_{py,0} - \varepsilon_{pp,0}) + E''_{p,0}(\varepsilon - \varepsilon_{py,0}) & \varepsilon_{py,0} < \varepsilon \le \varepsilon_{pu,cor} \\ 0 & \varepsilon > \varepsilon_{pu,cor} \end{cases}$$
$$\varepsilon_{pu,cor} \le \varepsilon_{py,0} \begin{cases} 0.33 \le \dfrac{P_{max}}{r_{outer}} < 0.86 \end{cases} \begin{cases} \varepsilon E_{p,0} & \varepsilon \le \varepsilon_{pp,0} \\ \varepsilon_{pp,0}E_{p,0} + E'_{p,0}(\varepsilon - \varepsilon_{pp,0}) & \varepsilon_{pp,0} < \varepsilon \le \varepsilon_{pu,cor} \\ 0 & \varepsilon > \varepsilon_{pu,cor} \end{cases} \tag{15}$$
$$0.86 \le \frac{P_{max}}{r_{outer}} < 2.00 \quad \begin{cases} \varepsilon E_{p,0} & \varepsilon \le \varepsilon_{pu,cor} \\ 0 & \varepsilon > \varepsilon_{pu,cor} \end{cases}$$

$$\varepsilon_{pu,cor} = \left[1 - 0.599\left(\frac{P_{max}}{r_{outer}} - 0.33\right)\right] \varepsilon_{py,0} \quad 0.33 \le \frac{P_{max}}{r_{outer}} \le 2.00 \tag{12}$$

Finally, adopting the same corroded samples considered for the definition of the decay relationship of the ultimate corroded strain, the decay of the residual cross-section of the corroded wire, $A_{w,cor}$, is defined as a function of the ratio P_{max}/r_{outer}, as shown in Figure 7. In detail, Equations (13) and (14) are determined by taking into account the same boundary limits of the ratio P_{max}/r_{outer} previously adopted in Equations (11) and (12).

$$A_{w,cor}(P_{max}) = \left[\left(1 - 0.303\frac{P_{max}}{r_{outer}}\right) A_{w,0}\right] \quad 0.00 < \frac{P_{max}}{r_{outer}} < 0.33 \tag{13}$$

17517648, 2023, 1, Downloaded from https://onlinelibrary.wiley.com/doi/10.1002/suco.202200170 by Politecnico Di Torino Sist. Bibl Del Polit Di Torino, Wiley Online Library on [06/06/2023]. See the Terms and Conditions (https://onlinelibrary.wiley.com/terms-and-conditions) on Wiley Online Library for rules of use; OA articles are governed by the applicable Creative Commons License

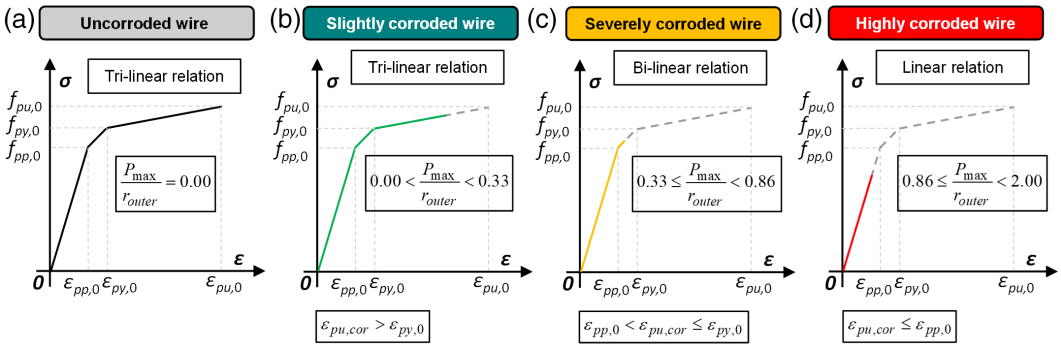

FIGURE 8 Mechanical response of a prestressing wire for different levels of corrosion: (a) uncorroded, (b) slightly corroded, (c) severely corroded, and (d) highly corroded wire. DIC, digital image correlation

approximately equal to 3/7 of the diameter of the external wire, ϕ_{outer}, as reported in Figures 6 and 8.

Finally, the overall mechanical response of a corroded prestressing strand is predicted through Equation (16) by assuming the equivalent spring model:

$$\sigma(\varepsilon) = \frac{\sigma_{w,max}(\varepsilon P_{max}) A_{w,outer,cor}(P_{max}) + 5 \cdot \sigma_{w,av}(\varepsilon P_{av}) A_{w,outer,cor}(P_{av}) + \sigma_{w,inner}(\varepsilon P_{inner}) A_{w,inner,cor}(P_{inner})}{\sum_{i=1}^{6}(A_{w,outer,0,i}) + A_{w,inner,0}} = \frac{\sigma_{w,max}(\varepsilon P_{max}) A_{w,outer,cor}(P_{max}) + 5 \cdot \sigma_{w,av}(\varepsilon P_{av}) A_{w,outer,cor}(P_{av}) + \sigma_{w,0}(\varepsilon) A_{w,inner,0}}{A_{strand,0}} \quad (16)$$

where $\sigma_{w,inner}(\varepsilon, P_{inner})$ and $A_{w,inner,cor}(P_{inner})$—in this case study—are assumed equal to $\sigma_{w,0}(\varepsilon)$ and $A_{w,inner,0}$ because the inner wire resulted uncorroded from experimental finding, that means a maximum penetration depth of the inner wire, P_{inner}, equal to 0.0, as highlighted in Figures 3 and 9.

As shown in Figure 9, the simplified version of the model sums the contributions of the seven wires, assuming these latter as springs working in parallel to the others. In particular, the springs that reproduce the behavior of the external wires, except for the most corroded one, are characterized by the same average penetration depth, P_{av}, and consequently fail simultaneously. Finally, the last wire that reaches the failure stage is the inner wire, which—in this particular case study—is assumed uncorroded and therefore will behave with larger ultimate strain if compared with the external corroded wires.

3.3.1 | Simplified expression for daily engineering assessment

In the previous section, the general formulation of the SCPS-model was described. Hereafter, a useful simplified expression that can be easily applied in the daily engineering assessment of corroded PC members will be introduced for the description of the entire failure sequence of a corroded strand. In detail, Equation (16) can further simplify by considering that: (i) the first conventional failure in the overall residual response of the corroded strand occurs in correspondence of the rupture of the most corroded wire, $\sigma_{w,max}(\varepsilon, P_{max})$, (Point 1 in Figure 9), (ii) the following ruptures involve the remaining five external wires and occur simultaneously because the latter are characterized by the same average penetration depth, $\sigma_{w,av}(\varepsilon, P_{av})$, (Point 2 in Figure 9), and (iii) the last rupture involve the inner wire that is characterized by an higher cross-section and in the particular case study results to be unaffected by corrosion deterioration—even if generally is governed by its inner penetration depth—$\sigma_{w,inner}(\varepsilon, P_{inner})$, (Point 3 in Figure 9).

17517648, 2023, 1, Downloaded from https://onlinelibrary.wiley.com/doi/10.1002/suco.202200170 by Politecnico Di Torino Sist. Bibl Del Polit Di Torino, Wiley Online Library on [06/06/2023]. See the Terms and Conditions (https://onlinelibrary.wiley.com/terms-and-conditions) on Wiley Online Library for rules of use; OA articles are governed by the applicable Creative Commons License

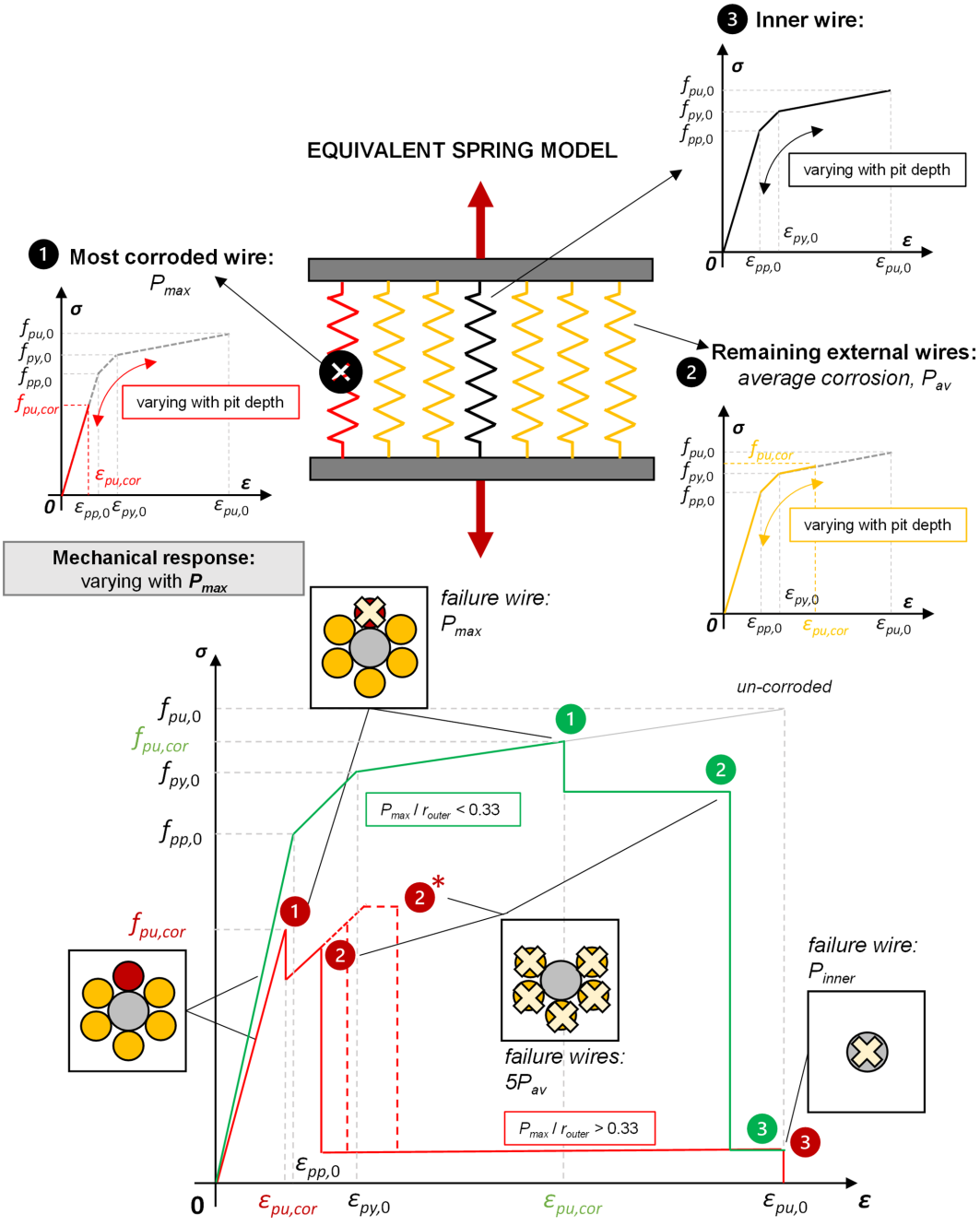

FIGURE 9 Mechanical response of a corroded prestressing strand: Equivalent spring model representation

The steps for the derivation of the crucial points of the stress–strain (tensile force-strain) relationship of a corroded strands, denoted as Points 1 and 2, are reported hereafter.

First, the ultimate corroded strength is predicted according to Equations (17) and (18):

Point 1: Failure of the most corroded wire.

$$\sigma_{w,\max}(\varepsilon, P_{\max}) = \begin{cases} 0.00 \le \dfrac{P_{\max}}{r_{\text{outer}}} < 0.33 & f_{\text{py},0} + E''_{\text{p},0}\left(\varepsilon_{\text{pu,cor}} - \varepsilon_{\text{py},0}\right) \quad \varepsilon_{\text{py},0} < \varepsilon_{\text{pu,cor}} \le \varepsilon_{\text{pu},0} \\ 0.33 \le \dfrac{P_{\max}}{r_{\text{outer}}} < 0.86 & f_{\text{pp},0} + E'_{\text{p},0}\left(\varepsilon_{\text{pu,cor}} - \varepsilon_{\text{pp},0}\right) \quad \varepsilon_{\text{pp},0} < \varepsilon_{\text{pu,cor}} \le \varepsilon_{\text{py},0} \\ 0.86 \le \dfrac{P_{\max}}{r_{\text{outer}}} < 2.00 & E_{\text{p},0}\varepsilon_{\text{pu,cor}} \quad \varepsilon_{\text{pu,cor}} < \varepsilon_{\text{pp},0} \end{cases} \tag{17}$$

17517648, 2023, 1, Downloaded from https://onlinelibrary.wiley.com/doi/10.1002/suco.202201170 by Politecnico Di Torino Sist. Bibl Del Polit Di Torino, Wiley Online Library on [06/06/2023]. See the Terms and Conditions (https://onlinelibrary.wiley.com/terms-and-conditions) on Wiley Online Library for rules of use; OA articles are governed by the applicable Creative Commons License

Point 2: Failure of the remaining five corroded external wires.

$$\sigma_{w,av}(\varepsilon, P_{av}) = \begin{cases} 0.00 \le \dfrac{P_{av}}{r_{outer}} < 0.33 & f_{py,0} + E''_{p,0}\left(\varepsilon_{pu,cor} - \varepsilon_{py,0}\right) \quad \varepsilon_{py,0} < \varepsilon_{pu,cor} \le \varepsilon_{pu,0} \\ 0.33 \le \dfrac{P_{av}}{r_{outer}} < 0.86 & f_{pp,0} + E'_{p,0}\left(\varepsilon_{pu,cor} - \varepsilon_{pp,0}\right) \quad \varepsilon_{pp,0} < \varepsilon_{pu,cor} \le \varepsilon_{py,0} \\ 0.86 \le \dfrac{P_{av}}{r_{outer}} < 2.00 & E_{p,0}\varepsilon_{pu,cor} \qquad \varepsilon_{pu,cor} < \varepsilon_{pp,0} \end{cases} \tag{18}$$

where P_{av} is predicted according to Equation (8), whereas the ultimate corroded strain, $\varepsilon_{pu,cor}$, is evaluated by adopting Equations (11) and (12) using the value of P_{max} or P_{av} for Points 1 and 2, respectively.

Thereafter, the residual mechanical response of the corroded prestressing strand is predicted through Equations (19) to (21) by assuming the equivalent spring model:

Point 1: strength of the strand in correspondence of the failure of the most corroded wire.

$$\begin{aligned} \sigma(\varepsilon) &= \frac{\sigma_{w,max}(\varepsilon P_{max}) A_{w,outer,cor}(P_{max}) + 5 \cdot \sigma_{w,av}(\varepsilon P_{av}) A_{w,outer,cor}(P_{av}) + \sigma_{w,0}(\varepsilon) A_{w,inner,cor}(P_{inner})}{\sum_{i=1}^{6}(A_{w,outer,0,i}) + A_{w,inner,0}} = \\ &= \frac{\sigma_{w,max}(\varepsilon P_{max}) \cdot \left(A_{w,outer,cor}(P_{max}) + 5 \cdot A_{w,outer,cor}(P_{av}) + A_{w,inner,0}\right)}{A_{strand,0}} = \\ &= \sigma_{w,max}(\varepsilon P_{max}) \frac{\left(A_{w,outer,cor}(P_{max}) + 5 \cdot A_{w,outer,cor}(P_{av}) + A_{w,inner,0}\right)}{A_{strand,0}} = \sigma_{w,max}(\varepsilon P_{max}) \alpha_{Acor} \end{aligned} \tag{19}$$

where $\sigma_{w,max}(\varepsilon, P_{max})$ is calculated through Equation (17), while α_{Acor} is a coefficient that estimate the dimensionless value of the residual cross-section of the overall strand as a function of the only parameter P_{max}/r_{outer} as given in Equation (20).

Point 2: strength of the strand in correspondence of the failure of the remaining five corroded external wires.

$$\sigma(\varepsilon) = \frac{\left(5 \cdot A_{w,outer,cor}(P_{av}) + A_{w,inner,0}\right)}{A_{strand,0}} = \sigma_{w,av}(\varepsilon, P_{av}) \alpha'_{Acor} \tag{21}$$

$$\alpha_{Acor}\left(\frac{P_{max}}{r_{outer}}\right) = \begin{cases} \dfrac{P_{max}}{r_{outer}} < 0.33 \\ \dfrac{A_{w,inner} + A_{w,outer}\left[\left(1 - 0.303\dfrac{P_{max}}{r_{outer}}\right) + 5\left(1 - 0.303\left(0.378\dfrac{P_{max}}{r_{outer}}^2 + 0.25\dfrac{P_{max}}{r_{outer}}\right)\right)\right]}{A_{strand,0}} \\ 0.33 < \dfrac{P_{max}}{r_{outer}} < 0.66 \\ \dfrac{A_{w,inner} + A_{w,outer}\left[\left(0.9 - 0.539\left(\dfrac{P_{max}}{r_{outer}} - 0.33\right)\right) + 5\left(1 - 0.303\left(0.378\dfrac{P_{max}}{r_{outer}}^2 + 0.25\dfrac{P_{max}}{r_{outer}}\right)\right)\right]}{A_{strand,0}} \\ \dfrac{P_{max}}{r_{outer}} > 0.66 \\ \dfrac{A_{w,inner} + A_{w,outer}\left[\left(0.9 - 0.539\left(\dfrac{P_{max}}{r_{outer}} - 0.33\right)\right) + 5\left(0.9 - 0.539\left(\left(0.378\dfrac{P_{max}}{r_{outer}}^2 + 0.25\dfrac{P_{max}}{r_{outer}}\right) - 0.33\right)\right)\right]}{A_{strand,0}} \end{cases} \tag{20}$$

17517648, 2023, 1, Downloaded from https://onlinelibrary.wiley.com/doi/10.1002/suco.202201170 by Politecnico Di Torino Sist. Bibl Del Polit Di Torino, Wiley Online Library on [06/06/2023]. See the Terms and Conditions (https://onlinelibrary.wiley.com/terms-and-conditions) on Wiley Online Library for rules of use; OA articles are governed by the applicable Creative Commons License

$$\alpha'_{\mathrm{Acor}}\left(\frac{P_{\max}}{r_{\mathrm{outer}}}\right)=\begin{cases}\dfrac{P_{\max}}{r_{\mathrm{outer}}}<0.66 \\ \dfrac{A_{\mathrm{w,inner}}+5A_{\mathrm{w,outer}}\left(1-0.303\left(0.378\frac{P_{\max}}{r_{\mathrm{outer}}}^{2}+0.25\dfrac{P_{\max}}{r_{\mathrm{outer}}}\right)\right)}{A_{\mathrm{strand,0}}} \\ \dfrac{P_{\max}}{r_{\mathrm{outer}}}>0.66 \\ \dfrac{A_{\mathrm{w,inner}}+5A_{\mathrm{w,outer}}\left(0.9-0.539\left(\left(0.378\frac{P_{\max}}{r_{\mathrm{outer}}}^{2}+0.25\dfrac{P_{\max}}{r_{\mathrm{outer}}}\right)-0.33\right)\right)}{A_{\mathrm{strand,0}}}\end{cases} \tag{22}$$

where $\sigma_{\mathrm{w,av}}(\varepsilon,\ P_{\mathrm{av}})$ is calculated through Equation (18), while α'_{Acor} is a coefficient that estimates the dimensionless value of the residual cross-section of the overall strand as a function of the only parameter $P_{\max}/r_{\mathrm{outer}}$ as given in Equation (22) where the cross-section of the most corroded wire, which failed after Point 1, is not considered.

Finally, the corresponding residual tensile force is calculated through Equations (23) and (24).

Point 1: tensile resistance of the strand in correspondence of the failure of the most corroded wire.

$$T_{\mathrm{pu,cor,analytical,1}}=\sigma_{\mathrm{w,max}}(\varepsilon,P_{\max})\alpha_{\mathrm{Acor}}A_{\mathrm{strand,0}} \tag{23}$$

Point 2: tensile resistance of the strand in correspondence of the failure of the remaining five corroded external wires.

$$T_{\mathrm{pu,cor,analytical,2}}=\sigma_{\mathrm{w,av}}(\varepsilon,P_{\mathrm{av}})\alpha'_{\mathrm{Acor}}A_{\mathrm{strand,0}} \tag{24}$$

4 | RESULTS AND DISCUSSION

The proposed stress–strain relationship for corroded prestressing strands is first validated through the comparison with experimental tensile tests coming from Franceschini et al.[17] and Jeon et al.[18] Then, the obtained results in terms of ultimate corroded strain and strength are statistically analyzed by evaluating the average (μ), the SD (σ), the coefficient of variation (CV), and the coefficient of correlation (CoC), respectively.

4.1 | Validation of the proposed model with experimental outcomes

Figure 10 shows the comparison of the predicted and the experimental stress–strain responses for specimens PB9-L(12–82), PB9-L(426–496), PB11-L(196–266), PB11-R (273–318), PB12-L(12–82), PB12-R(100–170), PB13-R(0–70), and PB14-R(2–72), resulting from the tensile tests previously analyzed,[17] whereas Figure 11 reports the validation of the SCPS-model against the experimental tensile test results belonging to the work carried out by Jeon et al.[18] for specimens CS2, CS3, CS6, CS7, CS8, and CS10. Based on the obtained results, despite the simplifications adopted compared and considering the complexity of the chloride-induced corrosion process, a significant agreement between the analytical curves and experimental outcomes is observed.

Since the failure of the most corroded wire is assumed as a critical point in the failure behavior of the overall corroded strand, the latter is identified in Figures 10 and 11 in order to compare the experimental and the analytical strength and tensile force values of each analyzed strand. Additionally, as previously pointed out the SCPS-model is able to also predict the overall behavior of the corroded strands after the first rupture of the most corroded wire. Therefore, the entire postpeak behavior governed by the resistance contributions provided by the remaining corroded wires is highlighted.

4.2 | Statistical analysis of results

To have a better overview of the applicability of the SCPS-model, the comparison between the analytical and experimental results in terms of ultimate strength and ultimate strain are reported in Figure 12a,b, respectively, where the dashed black line corresponds to the perfect matching between analytical prediction and experimental outcomes. Referring to Figure 12a, a high level of accuracy is obtained in the estimation of the ultimate corroded strength, $f_{\mathrm{pu,cor,analytical,1}}$, except for two samples. On the other hand, even if a satisfactory prediction is fulfilled in case of ultimate corroded strain in Figure 12b, a slightly wider scatter of the predicted values, $\varepsilon_{\mathrm{pu,cor,analytical,1}}$, is observed. Nevertheless, the analytical results are conservative, providing a safety margin in the prediction of the mechanical behavior of corroded prestressing strands—as confirmed by the ratio

17517648, 2023, 1, Downloaded from https://onlinelibrary.wiley.com/doi/10.1002/suco.202200170 by Politecnico Di Torino Sist. Bibl Del Polit Di Torino, Wiley Online Library on [06/06/2023]. See the Terms and Conditions (https://onlinelibrary.wiley.com/terms-and-conditions) on Wiley Online Library for rules of use; OA articles are governed by the applicable Creative Commons License

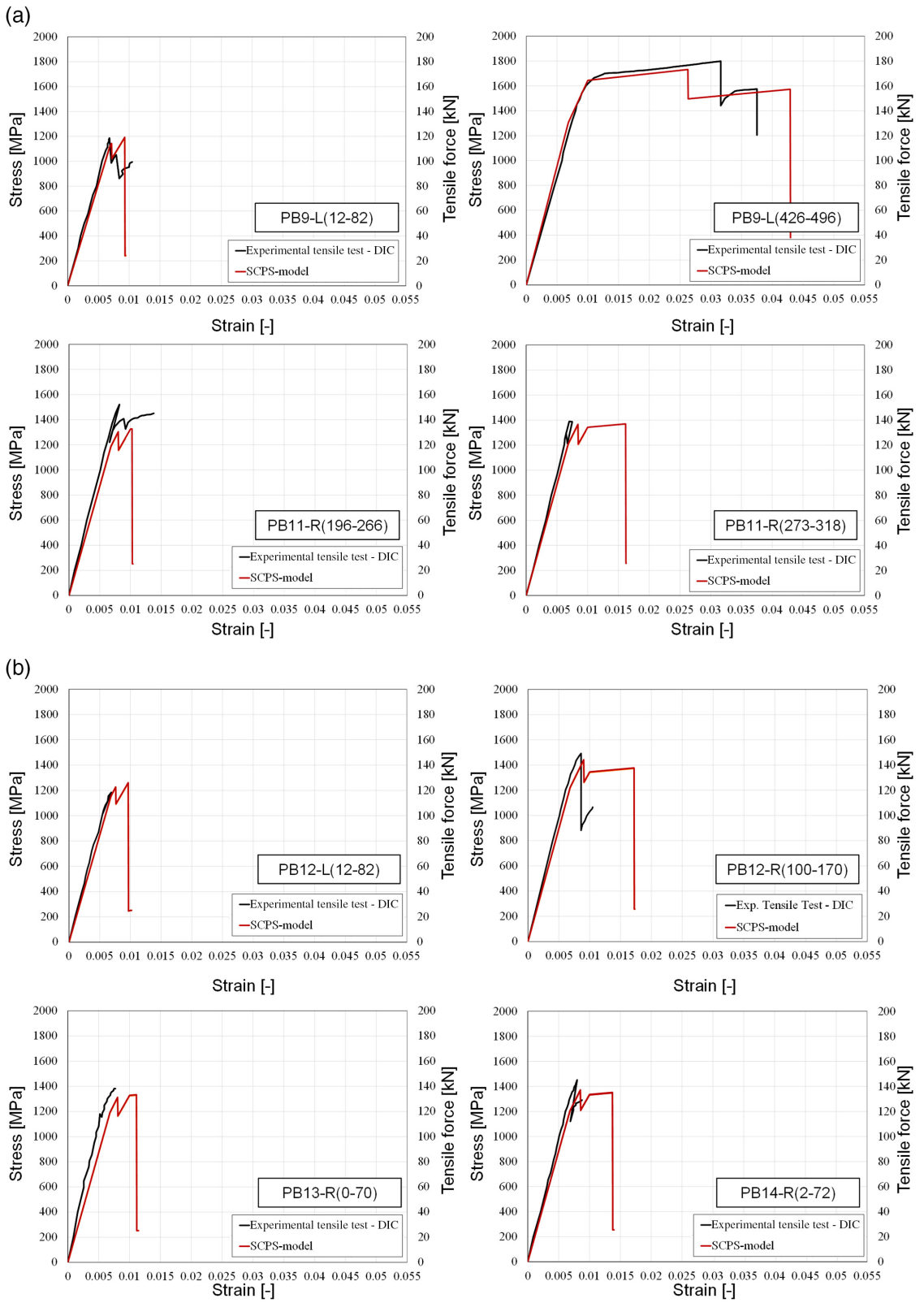

FIGURE 10 Validation of the SCPS-model with experimental outcomes from.[17]

$f_{pu,cor,exp}/f_{pu,cor,analytical,1}$ higher than 1.0. It is worth noting that this study takes into account all the experimental tensile tests outcomes available in the scientific literature that reports the parameters useful for the application and validation of the proposed SCPS-model (i.e., P_{max}/r_{outer}), as shown in Table 1. Nevertheless, additional experimental tensile tests on corroded prestressing strands are highly recommended to increase the available data, which are

17517648, 2023, 1, Downloaded from https://onlinelibrary.wiley.com/doi/10.1002/suco.202201170 by Politecnico Di Torino Sist. Bibl Del Polit Di Torino, Wiley Online Library on [06/06/2023]. See the Terms and Conditions (https://onlinelibrary.wiley.com/terms-and-conditions) on Wiley Online Library for rules of use; OA articles are governed by the applicable Creative Commons License

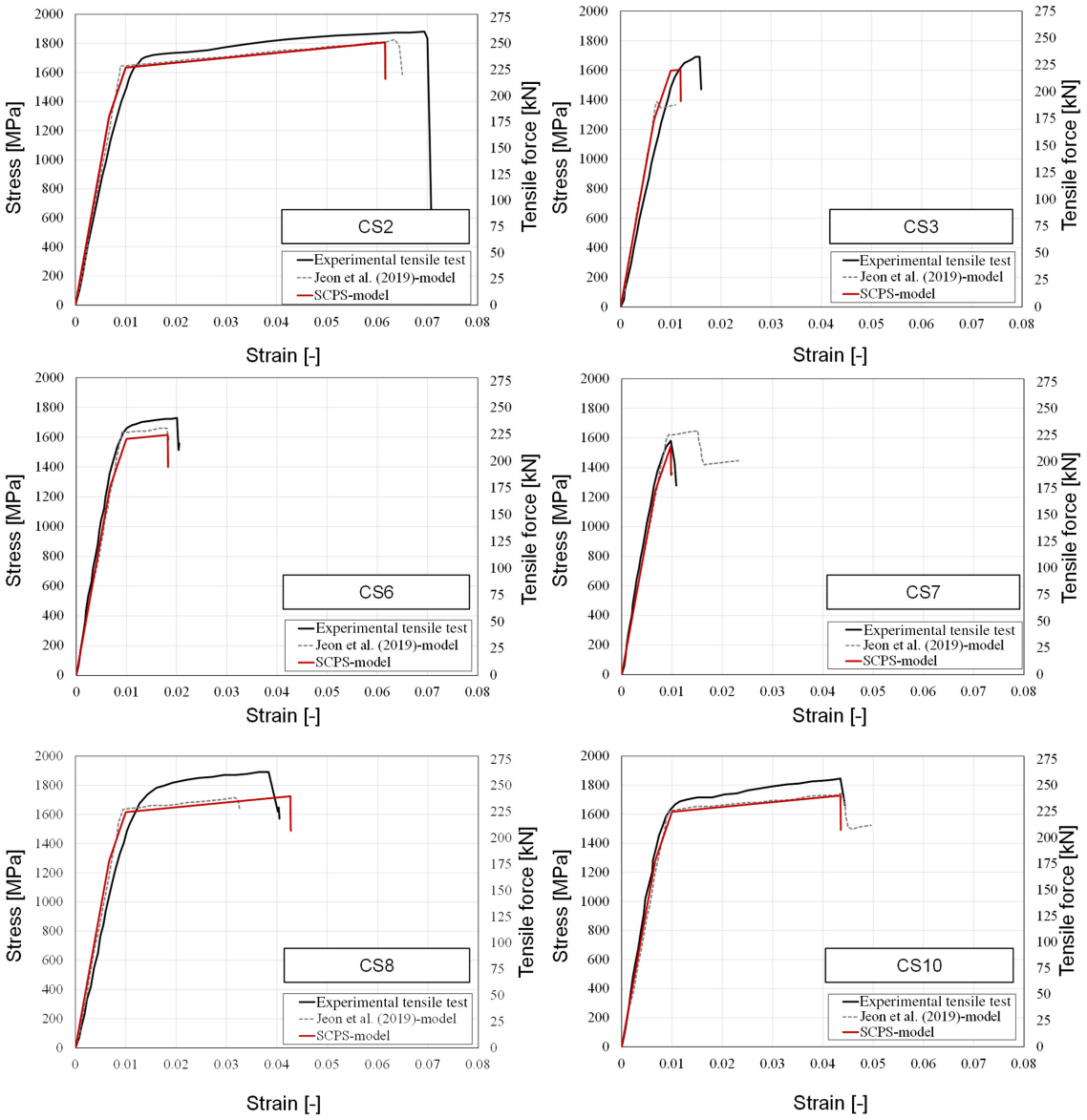

FIGURE 11 Validation of the SCPS-model with experimental outcomes coming from.[18]

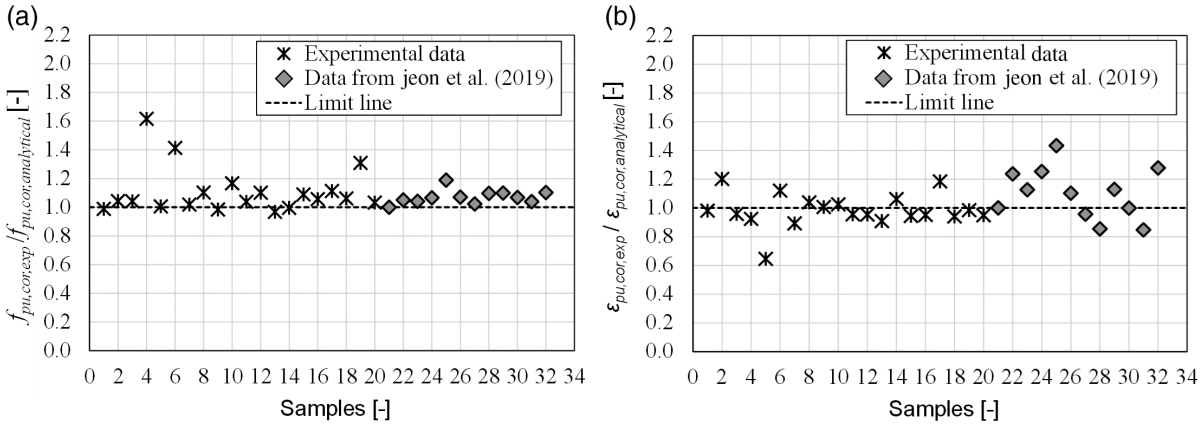

FIGURE 12 Comparison of experimental and analytical outcomes: (a) ultimate strength and (b) ultimate strain

17517648, 2023, 1, Downloaded from https://onlinelibrary.wiley.com/doi/10.1002/suco.202201170 by Politecnico Di Torino Sist. Bibl Del Polit Di Torino, Wiley Online Library on [06/06/2023]. See the Terms and Conditions (https://onlinelibrary.wiley.com/terms-and-conditions) on Wiley Online Library for rules of use; OA articles are governed by the applicable Creative Commons License

essential for the improvement and refinement of the statistical analysis carried out.

Finally, the dimensionless ratios of experimental and analytical results in terms of both ultimate strength and strain are evaluated and statistically treated in terms of average (μ), SD (σ), CV, and CoC. As highlighted in Table 3, the powerfulness of the SCPS-model is underlined by an average value, μ, close to 1.0 and a SD, σ, limited to 0.130 and 0.147 for ultimate strength and ultimate strain, respectively. Moreover, the accuracy of predictions is confirmed by the value of the CoC, that results equal to 0.942 and 0.979 for ultimate strength and ultimate strain, respectively.

5 | CONCLUSIONS

The study presents a simplified version of a constitutive law, named SCPS-model, for the prediction of the stress–strain response of corroded prestressing strands subjected to chloride-induced corrosion deterioration. To this aim, a total of 35 experimental tensile test outcomes coming from scientific literature are considered for the validation of the proposed model. According to the SCPS-model, the residual tensile response of a corroded prestressing strand is evaluated by adopting the equivalent spring model and its powerfulness consists in its dependency on a single input parameter, which is the maximum penetration depth of the most corroded wire. The model results to be independent from the usual parameters of the mass loss of the corroded strand or the cross-sectional loss of each corroded wire. Since the maximum penetration depth can be easily measured during in situ inspection, the application of the model in the daily engineering practice is promoted. A maximum penetration depth equal to 1/6 of the diameter of the external wire is established as the critical value at which the mechanical response of the corroded wire turns from ductile to brittle. Based on the obtained results and considering the adopted simplifications, the SCPS-model can properly predict the tensile response in terms of stress–strain curve (tensile force–strain curve) of a corroded prestressing strand with a margin of safety, as further confirmed by the statistical analysis carried out on the dimensionless ratios of ultimate strength and ultimate strain.

To support the use of the proposed model during engineering practice, future studies should address the identification of an operative procedure for sampling and measuring along the corroded length of the strand; indeed, the study of innovative instrumentation, such as micro portable laser scanners also complemented by software for maximum pit and wire radius estimation, should be promoted. Moreover, since stress corrosion could be a relevant phenomenon in corroded existing structures with longer useful life, a further research will be devoted to the application of the proposed methodology to monitored existing structures to validate if the latter phenomenon can be considered a conditioning factor for the proposed model.

ACKNOWLEDGEMENTS

Open Access Funding provided by Universita degli Studi di Parma within the CRUI-CARE Agreement.

CONFLICT OF INTEREST

The author declares that there is no conflict of interest that could be perceived as prejudicing the impartiality of the research reported.

DATA AVAILABILITY STATEMENT

The data that support the findings of this study are available from the corresponding author upon reasonable request.

ORCID

Lorenzo Franceschini https://orcid.org/0000-0003-4826-4163
Beatrice Belletti https://orcid.org/0000-0002-4382-9930
Francesco Tondolo https://orcid.org/0000-0003-0258-3054
Javier Sanchez Montero https://orcid.org/0000-0002-4334-0553

REFERENCES

1. United Nations Office for Disaster Risk Reduction (UNDRR). GAR: global assessment report on disaster risk reduction, Geneva, Switzerland; 2019. ISBN: 978-92-1-004180-5.
2. United Nations Office for Disaster Risk Reduction (UNDRR). Making critical infrastructure resilient: ensuring continuity of service policy and regulations in Europe and central Asia. Regional Office for Europe & Asia, Belgium; 2020.
3. European Committee for Standardization. Concrete – Part 1: Specification, performance, production and confirmity (European standard EN206-1). Brussels, Belgium: CEN; 2000.
4. Angst UM. Challenges and opportunities in corrosion of steel in concrete. Mater Struct. 2018;51(1):1–20. https://doi.org/10.1617/s11527-017-1131-6
5. Caprili S, Salvatore W. Cyclic behaviour of uncorroded and corroded steel reinforcing bars. Construct Build Mater. 2015;76:168–86. https://doi.org/10.1016/j.conbuildmat.2014.11.025
6. Caprili S, Salvatore W. Mechanical performance of steel reinforcing bars in uncorroded and corroded conditions. Data Brief. 2018;18:1677–95. https://doi.org/10.1016/j.dib.2018.04.072
7. Fernandez I, Bairán JM, Marí AR. Corrosion effects on the mechanical properties of reinforcing steel bars. Fatigue and σ-ε behavior. Construct Build Mater. 2015;101:772–83. https://doi.org/10.1016/j.conbuildmat.2015.10.139
8. Kashani MM, Alagheband P, Khan R, Davis S. Impact of corrosion on low-cycle fatigue degradation of reinforcing bars with the effect of inelastic buckling. Int J Fatigue. 2015;77:174–85. https://doi.org/10.1016/j.ijfatigue.2015.03.013
9. Kashani MM, Crewe AJ, Alexander NA. Nonlinear cyclic response of corrosion-damaged reinforcing bars with the effect of buckling. Construct Build Mater. 2013;41:388–400. https://doi.org/10.1016/j.conbuildmat.2012.12.011

17517648, 2023, 1, Downloaded from https://onlinelibrary.wiley.com/doi/10.1002/suco.202201170 by Politecnico Di Torino Sist. Bibl Del Polit Di Torino, Wiley Online Library on [06/06/2023]. See the Terms and Conditions (https://onlinelibrary.wiley.com/terms-and-conditions) on Wiley Online Library for rules of use; OA articles are governed by the applicable Creative Commons License

10. Li S, Tang H, Gui Q, Ma ZJ. Fatigue behavior of naturally corroded plain reinforcing bars. Construct Build Mater. 2017;152:933–42. https://doi.org/10.1016/j.conbuildmat.2017.06.173
11. Lu C, Yuan S, Cheng P, Liu R. Mechanical properties of corroded steel bars in pre-cracked concrete suffering from chloride attack. Construct Build Mater. 2016a;123:649–60.
12. Meda A, Mostosi S, Rinaldi Z, Riva P. Experimental evaluation of the corrosion influence on the cyclic behaviour of RC columns. Eng Struct. 2014;76:112–23. https://doi.org/10.1016/j.engstruct.2014.06.043
13. Ou YC, Susanto YT, Roh H. Tensile behavior of naturally and artificially corroded steel bars. Construct Build Mater. 2016;103:93–104.
14. Taha NA, Morsy M. Study of the behavior of corroded steel bar and convenient method of repairing. HBRC J. 2016;12(2):107–13. https://doi.org/10.1016/j.hbrcj.2014.11.004
15. Vanama RK, Ramakrishnan B. Improved degradation relations for the tensile properties of naturally and artificially corroded steel rebars. Construct Build Mater. 2020;249:118706. https://doi.org/10.1016/j.conbuildmat.2020.118706
16. Zhang W, Song X, Gu X, Li S. Tensile and fatigue behavior of corroded rebars. Construct Build Mater. 2012;34:409–17. https://doi.org/10.1016/j.conbuildmat.2012.02.071
17. Franceschini L, Vecchi F, Tondolo F, Belletti B, Montero SJ. Mechanical behaviour of corroded strands under chloride attack: a new constitutive law. Construct Build Mater. 2022;316:125872.
18. Jeon CH, Lee JB, Lon S, Shim CS. Equivalent material model of corroded prestressing steel strand. J Mater Res Technol. 2019;8(2):2450–60. https://doi.org/10.1016/j.jmrt.2019.02.010
19. Lu, Z., Li, F., & Zhao, Y. G. An investigation of degradation of mechanical behaviour of prestressing strands subjected to chloride attacking, 5th International Conference on Durability of Concrete Structures, Jun 30th – Jul 1st, 2016. Shenzhen University, Shenzhen, Guangdong Province, China; 2016b.
20. Wang L, Li T, Dai L, Chen W, Huang K. Corrosion morphology and mechanical behavior of corroded prestressing strands. J Adv Concrete Technol. 2020;18(10):545–57. https://doi.org/10.3151/jact.18.545
21. Zhang X, Wang L, Zhang J, Liu Y. Corrosion-induced flexural behavior degradation of locally ungrouted post-tensioned concrete beams. Construct Build Mater. 2017;134:7–17. https://doi.org/10.1016/j.conbuildmat.2016.12.140
22. Zhang WP, Li CK, Gu XL, Zeng YH. Variability in cross-sectional areas and tensile properties of corroded prestressing wires. Construct Build Mater. 2019;228:1–11. https://doi.org/10.1016/j.conbuildmat.2019.116830
23. American Society for Testing and Materials. ASTM G1-03. Standard practice for preparing, cleaning, and evaluating corrosion test specimens. West Conshohocken, PA: ASTM International; (2011).
24. Liu X, Zhang W, Gu X, Zeng Y. Degradation of mechanical behavior of corroded prestressing wires subjected to high-cycle fatigue loading. J Bridge Eng. 2017;22(5):04017004. https://doi.org/10.1061/(asce)be.1943-5592.0001030
25. Yoo CH, Park YC, Kim HK. Section loss in naturally corroded 7-wire steel strands in external tendons. Struct Infrastruct Eng. 2020;16(11):1593–603. https://doi.org/10.1080/15732479.2020.1714668
26. Val DV, Melchers ER. Reliability of deteriorating RC slab bridges. J Struct Eng. 1997;123(12):1638–44.
27. Hartt WH, Lee SK. Projecting corrosion induced bridge tendon failure resulting from deficient grout: part I - model development and example results. NACE Int Corros Conf Ser. 2016;1(8):448–59.
28. Belletti B, Rodríguez J, Andrade C, Franceschini L, Sánchez Montero J, Vecchi F. Experimental tests on shear capacity of naturally corroded prestressed beams. Struct Concr. 2020;21(5):1777–93. https://doi.org/10.1002/suco.202000205
29. Vecchi, F., Belletti, B., Franceschini, L., Andrade, C., Rodriguez, J., & Montero, S. J. Flexural tests on prestressed beams exposed to natural chloride action, 5th International Conference on Durability of Concrete Structures, Jun 30th – Jul 1st, 2016. Shenzhen University, Shenzhen, Guangdong Province, China; 2021a.
30. Vecchi F, Franceschini L, Tondolo F, Belletti B, Sánchez Montero J, Minetola P. Corrosion morphology of prestressing steel strands in naturally corroded PC beams. Construct Build Mater. 2021b;296:123720. https://doi.org/10.1016/j.conbuildmat.2021.123720
31. Blaber J, Adair B, Antoniou A. Ncorr: open-source 2D digital image correlation Matlab software. Exp Mech. 2015;55(6):1105–22. https://doi.org/10.1007/s11340-015-0009-1
32. Schreier H, Orteu J-J, Sutton MA. Image correlation for shape, motion and deformation measurements: Basic concepts, theory and applications. New York, NY: Springer; 2009.
33. Joint Committee of Structural Safety. JCSS Probabilistic Model Code - Part 3: Resistance Models; 2001.
34. American Society for Testing and Materials. ASTM a 421. Uncoated stress-relieved steel wire for prestressed concrete. ASTM a 722. Uncoated high-strength steel bar for prestressing concrete. Philadelphia: American Society for Testing and Materials; 2015.

AUTHOR BIOGRAPHIES

Lorenzo Franceschini
Department of Engineering and Architecture, University of Parma, Parco Area delle Scienze 181/A, 43124 Parma, Italy
lorenzo.franceschini@unipr.it

Beatrice Belletti
Department of Engineering and Architecture, University of Parma, Italy
beatrice.belletti@unipr.it

Francesco Tondolo
Department of Structural, Geotechnical and Building Engineering (DISEG), Politecnico di Torino, Torino, Italy
francesco.tondolo@polito.it

17517648, 2023, 1, Downloaded from https://onlinelibrary.wiley.com/doi/10.1002/suco.202201170 by Politecnico Di Torino Sist. Bibl Del Polit Di Torino, Wiley Online Library on [06/06/2023]. See the Terms and Conditions (https://onlinelibrary.wiley.com/terms-and-conditions) on Wiley Online Library for rules of use; OA articles are governed by the applicable Creative Commons License

Javier Sanchez
CSIC – Instituto de Ciencias de la Construction Eduardo Torroja (IETCC), Madrid, Spain
javier.sanchez@csic.es

How to cite this article: Franceschini L, Belletti B, Tondolo F, Sanchez Montero J. A simplified stress–strain relationship for the mechanical behavior of corroded prestressing strands: The SCPS-model. Structural Concrete. 2023;24(1):189–210. https://doi.org/10.1002/suco.202200170

17517648, 2023, 1, Downloaded from https://onlinelibrary.wiley.com/doi/10.1002/suco.202200170 by Politecnico Di Torino Sist. Bibl Del Polit Di Torino, Wiley Online Library on [06/06/2023]. See the Terms and Conditions (https://onlinelibrary.wiley.com/terms-and-conditions) on Wiley Online Library for rules of use; OA articles are governed by the applicable Creative Commons License